의학박사 학위논문

Role of transglutaminase 2 in acute colitis and skeletal muscle atrophy

급성 장염과 근위축증에서의 트랜스글루타미네이즈 2 의 역할

2016 년 8 월

서울대학교 대학원

의과학과 의과학전공

손 영 훈

A thesis of the Degree of Doctor of Philosophy

급성 장염과 근위축증에서의 트랜스글루타미네이즈 2 의 역할

Role of transglutaminase 2 in acute colitis and skeletal muscle atrophy

August 2016

The Department of Biomedical Sciences,
Seoul National University
College of Medicine
Young Hoon Son

Abstract

Role of transglutaminase 2 in acute colitis and skeletal muscle atrophy

Young Hoon, Son
Department of Biochemistry and Molecular Biology
Seoul National University college of Medicine

Transglutaminase 2 (TG2) is an enzyme that catalyzes post-translational modification including crosslinking, polyamination, and deamidation of proteins. TG2 is ubiquitously expressed and known to be involved in the pathogenesis of various diseases such as cataract, fibrosis, and cancer.

In the first part of this study, since TG2 is required to trigger inflammation via the induction of T_H17 cell differentiation in response to tissue damage, role of TG2 in inflammatory bowel disease, which is thought to be a T_H17 cell-associated disease, was investigated using dextran sulfate sodium (DSS)-induced colitis. DSS-treated $TG2^{-/-}$ mice showed no significant differences in changes of body weight, colon length, morphology, immune cell infiltration, and *in vivo* intestinal permeability, but showed higher mortality compared with wild-type. These results indicate that TG2 is dispensable but required for the survival of mice in dextran sulfate sodium-induced colitis

In the second part of this study, insulin/IGF1 signaling pathway impaired by steroid hormone was investigated using cellular and mouse models of dexamethasone-induced muscle atrophy. Dexamethasone-treated C2C12 myotubes showed decreased caveolin-1 protein and mRNA that lead to reduction in insulin receptor and IR substrate1 levels. These results indicate that caveolin-1 is a glucocorticoid target gene that links glucocorticoid signaling to the insulin signaling pathway.

In the third part of this study, role of TG2 in skeletal muscle homeostasis was investigated to explain the impairment of exercise ability of $TG2^{-/-}$ mice. Gastrocnemius (GA) muscle from $TG2^{-/-}$ mice showed a significant reduction

of muscle fiber size. Analyses of insulin/IGF signaling pathway in GA muscle revealed that protein level of PDK1 was decreased even though increased level of upstream PI3K. Using C2C12 myotubes, promoter analysis of PDK1 gene showed that treatment with inhibitor and siRNA of TG2 suppresses the reporter activity of c-Jun responsive element. Western blot and real-time RT-PCR analysis demonstrated that TG2 regulates the level of c-Jun protein, but not of mRNA through inhibition of proteasomal degradation of c-Jun. These results indicate that TG2 play a role in the maintenance of skeletal muscle homeostasis.

Keywords: transglutaminase 2, muscle atrophy, C2C12, dexamethasone, dextran sulfate sodium, insulin/IGF signaling pathway

Student Number: 2009-31109

CONTENTS

LIST OF FIGURES AND TABLES

Chapter 1

Chapter 2

Chapter 3

CHAPTER 1

Transglutaminase 2 is dispensable but required for the survival of mice in dextran sulfate sodium-induced colitis

1. Introduction

Transglutaminase 2 (TG2) is an enzyme that catalyzes the formation of crosslinked, polyaminated, or deamidated proteins (1). It is ubiquitously expressed in almost all human tissues and localized at cytosol, nucleus, mitochondria, cellular membrane and extracellular matrix (2). TG2 is inactive under normal condition, however, it is activated under pathological conditions including inflammation, injury, oxidative stress and hypoxia (3-5). Abnormal TG2 activity has been proposed to be a pathogenic factor of various diseases including cataract, fibrosis, and cancer (1).

A growing body of evidence suggests that TG2 also plays central roles in the pathogeneses of various inflammatory disorders (1, 6). TG2-catalyzed deamidation of dietary gluten peptide in small intestine is thought to be an essential event in the pathogenesis of celiac disease which is an intestinal autoimmune disease (7, 8). Deamidated gluten peptides present high binding affinity to the celiac disease-associated human leukocyte antigens (HLAs), HLA-DQ2 and HLA–DQ8, promoting gluten-mediated T cell activation (7). Besides, an autoantibody reactive to TG2 is produced by new epitope probably generated from its self-crosslinking product with gluten peptide in celiac disease patients (8). On the other hand, TG2 has been reported to potentiate intracellular inflammatory responses rendering T cells to differentiate into T helper 17 (Th17) cells which play a pivotal role in the pathogenesis of autoimmune diseases including bleomycin-induced lung fibrosis and experimental autoimmune encephalomyelitis (EAE) (9, 10). Bleomycin-stimulated TG2 activity up-regulated Th17 cell population by promoting nuclear factor κ-light-chain-enhancer of activated B cells (NF-κB) activation in lung epithelial cells, increasing the expression levels of interleukin-6 (IL-6) which is a crucial cytokine for the induction of Th17 cells (9). TG2 is also known to be involved in celiac disease, sepsis, and cystic fibrosis through modulation of NF-κB signaling by crosslinking and inactivating of NF-κB inhibitor α (IκBα) and peroxisome proliferator-activated receptor γ (PPARγ) (11-13). TG2 thus seems to be a general immunological modulator in

inflammatory diseases.

Inflammatory bowel disease (IBD), chiefly consisting of Crohn's disease (CD) and ulcerative colitis (UC) is an intestinal immune-mediated disorder (14, 15). It is thought to be the consequence through complex crosstalk between immune cells, epithelial cells, endothelial cells, stromal cells and luminal substances including enteric bacteria or dietary antigens in gastrointestinal track (14, 15). Although it has been suggested that polygenetic factors are complexly associated with the pathogenesis of IBD (16), genome-wide association studies (GWAS) in IBD emphasized the importance of the Th17 pathway and the NF-κB pathway through correlation with polymorphisms of genes encoding IL23R, TYK2, JAK2, STAT3, and CCR6 and genes encoding REL, TNFAIP3 and NFKB1, respectively (17-19). Besides, intriguingly, TG2 autoantibody has been reported to be found in serum of UC or CD patients (20), suggesting that intestinal TG2 may also generates neo-epitopes through its activity in IBD patients. Taken together, these data render us to hypothesize that TG2 might be involved in the pathogenesis of IBD.

In this study, to our knowledge, we for the first time investigated role of TG2 in IBD pathogenesis by applying dextran sulphate sodium (DSS)-induced colitis model to TG2 knockout ($TG2^{-/-}$) mice. DSS is thought to induce colitis through its toxic effect on intestinal epithelial cells, leading enteric commensal bacteria to penetrate epithelial cells and trigger intestinal inflammation (21) or the direct effect on the activation of dendritic cells (22). Oral consumption of DSS in drinking water is well known to trigger colitis in many experimental animals including mouse, rat, guinea pig and hamster that resembles the clinical and histological features of IBD, particularly UC (23). The colitis is dependent on the administrated DSS concentration and duration and can be recovered to normal status after withdrawal of DSS in drinking water to mimic remission of IBD (23). Here, we demonstrate that mouse colonic TG2 is activated by administration of DSS, however, the clinical and histological colonic inflammatory parameters in $TG2^{-/-}$ mice fed DSS show no significant difference compared with those in wild type ($TG2^{+/+}$) mice. Our results indicate that TG2 has no crucial role in acute DSS-induced colitis.

2. Materials and Methods

2-1. Mice

C57BL/6J mice were obtained from The Jackson Laboratory. $TG2^{-/-}$ mice were backcrossed to C57BL/6J mice for 10 generations (N10). Mice were kept in essentially specific pathogen-free environment at the animal facility of Seoul National University College of Medicine. All animal experiments were carried out with the approval of the Institutional Animal Care and Use Committee at Seoul National University.

2-2. Induction of colitis by dextran sulfate sodium (DSS)

DSS-induce mouse colitis model was applied in $TG2^{+/+}$ and $TG2^{-/-}$ mice matched of gender and age as described previously [24]. 14-wk-old mice were used for experiments. They were kept under a thermostatic and photoperiodic control (25°C and 12:12 h light-dark cycle, respectively). They were allowed to eat gluten-free standard mouse chow and filtered tap water ad libitum and adapt to these conditions for at least 14 days before inclusion in the experiments. Colitis was generated by administration of the DSS (36,000–50,000 Da; MP Biomedicals) dissolved in the autoclaved drinking water (2 and 3.5% wt/vol). Mice were treated with DSS or plain water for the indicated days. The mean water consumption was calculated by measurement for each group.

2-3. Clinical analysis

Progress of colitis was monitored by examination for weight loss, stool consistency, rectal bleeding, hunched posture, and mortality every day or every other day for each mouse during the treatment period. Five or ten days after the treatment of DSS-water, mice were euthanized by CO_2. The intact colon was detached from the caecum to the anus and taken a picture. The length of the colon was measured, and the colon was opened by incision and flushed with cold PBS for removal of fecal materials. Tissue gained from each colon was processed for subsequent analysis.

2-4. Histological evaluation of colonic lesions

Proximal and distal sections of colon were fixed with 4% paraformaldehyde, embedded in paraffin, and stained with H&E for the morphological evaluation. The histopathological changes were analyzed for these microscopic sections as described previously, according to the severity of the induced damage.

2-5. MPO assay

MPO activity was assessed to evaluate the extent of neutrophil infiltration into inflamed colonic lesion . Colon specimens were homogenized with 20 volumes of 50 mM phosphate buffer (pH 6.0) containing 0.5% hexadecyltrimethyl ammonium bromide (Sigma-Aldrich, St. Louis, MO) using Precellys 24 (Bertin technologies) and sonicated for 10 s. Homogenates were freeze-thawed three times, and then centrifuged at 14,000 rpm for 15 min, 4°C. 14 μl of supernatant was mixed with a solution of 1 mg/ml o-dianisidine hydrochloride (Sigma-Aldrich, ST. Louis, MO) and 0.0005% hydrogen peroxide. MPO activity was measured spectrophotometrically as the change in absorbance at 460 nm. One unit of MPO activity was defined as the amount that was the absorbance change per minute at 25°C in the reaction with 1 μmol peroxidase.

2-6. *In vivo* intestinal permeability

To assess barrier function, in vivo permeability assay was carried out using a FITC-dextran, as described with slight modification. Briefly, mice were housed without food and water for 4 hours and then orally gavaged with 0.6 g/kg of FITC-dextran (MW 3,000–5,000; Sigma-Aldrich) as a permeability tracer. After 4 hours, mice were euthanized and serum was collected. Fluorescence intensity of each sample was evaluated using Infinite^{TM} M200 (excitation at 492 nm and emission at 525 nm, TECAN). FITC-dextran concentrations in serum were calculated from standard curves generated by serial dilution of FITC dextran (0, 64, 320, 1600, 8000, 40000 ng/ml).

2-7. Real-time PCR

Whole colons collected from euthanized mice were washed to remove fecal

matter and then divided with proximal and distal colon. Total RNA was extracted using TRIzol (Invitrogen, Carlsbad, CA) from the samples and then reverse transcribed using SuperScript® II Reverse Transcriptase (Invitrogen, Carlsbad, CA). Real-time PCR was performed with KAPA SYBR® FAST qPCR Kit (Kapabiosystems) using a CFX96TM Real-Time system (Bio-Rad). The following specific primers were used [24]: 34B4, 5'-TCCAGGC TTTGGGCATCA-3' (forward) and 5'-CTTTATCAGCTGCAC ATCACTCAGA-3' (reverse); TNFα, 5'-AGGCTGCCCCGACTACGT-3' (forward) and 5'-GACTTTCTCCTGGTATGAGATAGCAAA-3' (reverse); IFNγ, 5'-CAGCAACAGCAAGGCGAAA-3' (forward) and 5'-CTGG ACCTGTGGGTTGTTGAC-3' (reverse); IL-1β, 5'-TCGCTCAGGGT CACAAGAAA-3' (forward) and 5'-CATCAGAGGCAAGGAGGAAAAC-3' (reverse); IL-6-ACAAGTCGGAGGCTTAATTACACAT-3' (forward) and 5'-TGCCATTGCACAACTCTTTT-3' (reverse); KC, 5'-CTTGAAGGTGTT GCCCTCAG-3' (forward) and 5'-TGGGGACACCTTTTAGCATC-3' (reverse); IL-10, 5'-GGTTGCCAAGCCTTATCGGA-3' (forward) and 5'-AC CTGCTCCACTGCCTTGCT-3' (reverse); IL-12, 5'-AGACCCTGCCCATT GAACTG-3' (forward) and 5'-GAAGCTGGTGCTGTAGTTCTCATATTT-3' (reverse); , 5'-GGCAAGGCTAACTGACCTGGAAAGG-3' (forward) and 5'-ACAGCGAGGCACATCAGGTACGA-3' (reverse). mRNA expression level was determined by the $2^{-\Delta\Delta Ct}$ method and normalized or compared to 34B4 levels. The results are given as relative fold compared to control samples.

2-8. Statistical Analysis

We calculated *P* values with GraphPad software (Prism 5) using two-way ANOVA followed by Bonferroni post-tests to compare individual means in the data of body weight changes, colon length shortness, MPO activity, FITC-dextran permeability, and real-time PCR. *P* values of the survival rate data were analyzed using Log-rank test.

3. Results

3-1. Colonic TG2 activation in DSS-induced colitis mouse model

We first analyzed TG2 expression level and *in situ* TG activity in colon samples of $TG2^{+/+}$ and $TG2^{-/-}$ mice using confocal microscopy. We observed that TG2 was majorly expressed in lamina propria (LP), muscularis mucosae (MM) and overall submucosa (SM) of $TG2^{+/+}$ mice colon (Fig. 1, NT of $TG2^{+/+}$) and slightly detected in epithelial cells including columnar absorptive cells (CA) and goblet cells (G). However, we could hardly detect transglutaminase (TG) activity in colon of untreated TG2+/+ mice. In colon of 3.5% DSS-treated $TG2^{+/+}$ mice for 5 days, TG2 expression levels were higher than those in non-treated $TG2^{+/+}$ colon and its activity was appeared in whole colon area (Fig. 1, 3.5% DSS of $TG2^{+/+}$). Intriguingly, TG2 activity in CA of DSS-treated $TG2^{+/+}$ mice were high in spite of low TG2 expression levels. On the other hand, we could not observe any TG activity in colon of DSS-treated $TG2^{-/-}$ mice (Fig. 1, 3.5% DSS of $TG2^{-/-}$), indicating that TG2 is the sole TG isotype to contribute DSS-induced colonic TG activity.

3-2. TG2 role in mouse body weight change and survival rate during DSS administration

To test whether TG2 is involved in DSS-induced experimental colitis, we next analyzed body weight change and survival rate in DSS-treated $TG2^{+/+}$ and $TG2^{-/-}$ mice to investigate the role of TG2 in DSS-induced acute colitis model. DSS-supplemented water intake did not differ between $TG2^{+/+}$ and $TG2^{-/-}$ mice (data not shown). Both mice groups showed diarrhea, rectal bleeding and body weight loss by DSS treatment, suggesting that the experimental colitis model was well established. However, we observed that there were no significant differences in the extent of diarrhea and rectal bleeding (data not shown) and body weight change (Fig. 2A) between $TG2^{+/+}$ and $TG2^{-/-}$ mice treated with 2% DSS for 7 days. Both $TG2^{+/+}$ and $TG2^{-/-}$ mice lost weight from 7th day after initiation of the administration with almost identical manner. On day 10, their body weight significantly decreased down to 84% compared with that of

untreated control mice, then began to recover on day 11 and returned to normalcy on day 18 (Fig. 2A). Although mice treated with 2% DSS for 7 days showed lethality rate of 12.5% (1 out of 8) on different days, there was no significant difference between $TG2^{+/+}$ and $TG2^{-/-}$ mice (Fig. 2B). We next applied mice to more severe colitis conditions through treatment of 2% DSS for 8 days or 3.5% DSS for 6 days. Body weight changes did not differ between $TG2^{+/+}$ and $TG2^{-/-}$ under these conditions (Fig. 2C). Interestingly, $TG2^{-/-}$ mice were significantly more lethal under these severe colitis conditions compared with $TG2^{+/+}$ mice (Fig. 2D).

3-3. Analysis of additional colitis parameters in $TG2^{+/+}$ and $TG2^{-/-}$ mice treated with DSS

We further evaluated the well-established other colitis parameters in DSS-medicated $TG2^{+/+}$ and $TG2^{-/-}$ mice including colon length shortening, histological changes, myeloperoxidase (MPO) activity and *in vivo* transepithelial permeability. For these experiments, mice colitis was induced by treatment of 2% and 3.5% DSS-water according to the following procedures. 2% DSS-induced mouse colitis was prepared by treatment with 2% DSS-water for 8 days and subsequently fed with plain water for 2 days. 3.5% DSS-induced mouse colitis was prepared by feeding 3.5% DSS-water for 5 days. DSS-treated mice were sacrificed at the final days and then analyzed for colitis parameters. We found that colon length of $TG2^{-/-}$ mice treated with 2% and 3.5% DSS-water was significantly reduced as around 64% and 88%, respectively, compared with untreated mice, but there was no significant difference compared to DSS-treated $TG2^{+/+}$ colon length (Fig. 3). We then obtained fixed proximal and distal colon sections and stained them with hematoxylin and eosin (H&E) dye for histological analysis. As shown in Fig. 4, proximal and distal colon sections from water-fed $TG2^{-/-}$ mice featured normal architectures with the intact epithelium, regular crypt length, and no ulcers or erosions like colon sections from control $TG2^{+/+}$ mice. Colon sections from 2.5% or 3% DSS-water treated $TG2^{+/+}$ and $TG2^{-/-}$ mice showed severe inflammatory lesions characterized by loss of crypts and extensive infiltration of immune cells including neutrophils

and lymphocytes throughout mucosa. This inflammatory response was more pronounced in distal colons sections than proximal colon sections from DSS-water treated mice, however, there was no distinguishable difference between $TG2^{+/+}$ and $TG2^{-/-}$ mice colon sections (Fig. 5). To quantify the extent of neutrophil infiltration into colonic mucosa, we measured colonic MPO activity. MPO activity levels were significantly higher in distal colon samples of 2% or 3.5% DSS-water fed $TG2^{+/+}$ mice than those of plain water fed $TG2^{+/+}$ mice (Fig. 5). Similar patterns were observed in $TG2^{-/-}$ mice colon samples. However, no significant difference existed between $TG2^{+/+}$ and $TG2^{-/-}$ mice groups. Because epithelial barrier function loss is considered as the critical event in inflammatory bowel disease as well as DSS-induced experimental colitis, we next assayed *in vivo* permeability of colonic epithelial barrier using a fluorescein isothiocyanate (FITC)-labeled dextran method as described in Materials and Methods. DSS-water treated mice groups significantly showed increased serum FITC-dextran levels compared to plain water treated mice (Fig. 6). However, in all conditions FITC-dextran levels in serums of $TG2^{-/-}$ mice did not differ from those of $TG2^{+/+}$ mice. Taken together, these results suggest that TG2 does not associated with the regulation of colitis-related clinical parameters in DSS-induced experimental colitis mouse model.

3-4. TG2 involvement in the expression levels of colonic inflammatory mediators in DSS-induced colitis

In the process of IBD including DSS-induced experimental colitis, inflammatory cytokines produced by infiltrated immune cells and damaged epithelial cells in intestine play a key role . Thus, we analyzed the levels of inflammatory cytokines and a chemokine in distal colon samples obtained from 3.5% DSS water-fed $TG2^{+/+}$ and $TG2^{-/-}$ mice using real-time PCR method as described in Materials and Methods. As shown in Fig. 7A, IL-6 mRNA levels were dramatically increased in colons of both groups by DSS treatment for a period of 5 days but significantly 2.2-fold higher in colons of $TG2^{+/+}$ mice than those of $TG2^{-/-}$ mice. In contrast, tumor necrosis factor α (TNFα) mRNA levels were gradually risen during DSS treatment in colons of both groups but colons

of $TG2^{-/-}$ mice showed 1.6- and 1.3-fold elevated levels compared to those of $TG2^{+/+}$ mice on day 3 and 5, respectively (Fig. 7E). DSS raised mRNA expression levels of keratinocyte chemoattractant (KC) (Fig. 7F), IL-10 (Fig. 7G), and IL-17A (Fig. 7B) 1.8-, 2.6-, and 11.3-fold higher in $TG2^{-/-}$ colons with peaks on day 3 than $TG2^{+/+}$ colons, respectively. Notably, mRNA levels of RAR-related orphan receptor γt (RORγt) which is a master regulatory transcription factor of the Th17 pathway including IL-17A increased 6.6-fold higher in $TG2^{-/-}$ mice colon than $TG2^{+/+}$ mice colon. This result indicates that the population of Th17 cells or innate lymphoid cells 3 (ILC3) cells generating IL-17A in intestine (24) was higher in $TG2^{-/-}$ colon than $TG2^{+/+}$ colon. On the other hand, mRNA levels of IL-17F (Fig. 7F), IL-12 (Fig. 7G), and interferon γ (IFNγ) (Fig. 7H) were similarly increased by DSS treatment in both groups. In addition, we could not observe significant changes of IL-1β mRNA level by DSS stimulation in both group mice colons (Fig. 7I). These data suggest that the expression levels of inflammatory mediators are differently regulated in colons of $TG2^{+/+}$ and $TG2^{-/-}$ mice fed with DSS water.

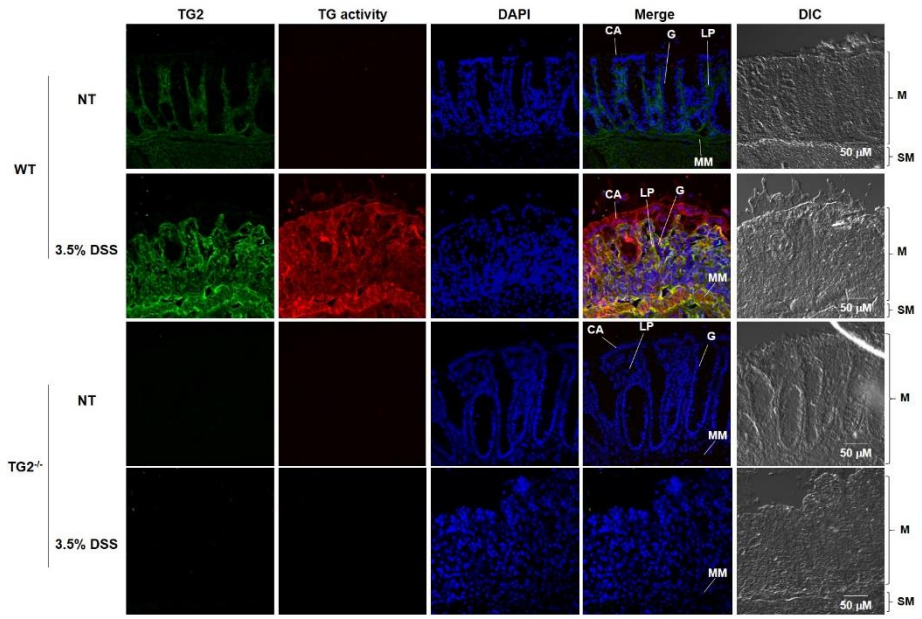

Figure 1. ***In vivo*** **intestinal transglutaminase activity in colon inflamed by DSS treatment.** Mice treated with drinking water containing 3.5% DSS for 5 days were

intraperitoneally injected with 100 mg/kg biotin-amido-pentylamine, and then sacrificed after 3 h. Colons were cryosectioned and then were stained with TG2 antibody, Texas Red-conjugated streptavidin, and DAPI for TG2, TG activity, and nucleus detection, respectively. M, Mucosa; SM, Submucosa; MM, Muscularis mucosae; CA, Columnar Absorptive cells; G, Goblet cells; LP, Lamina propria.

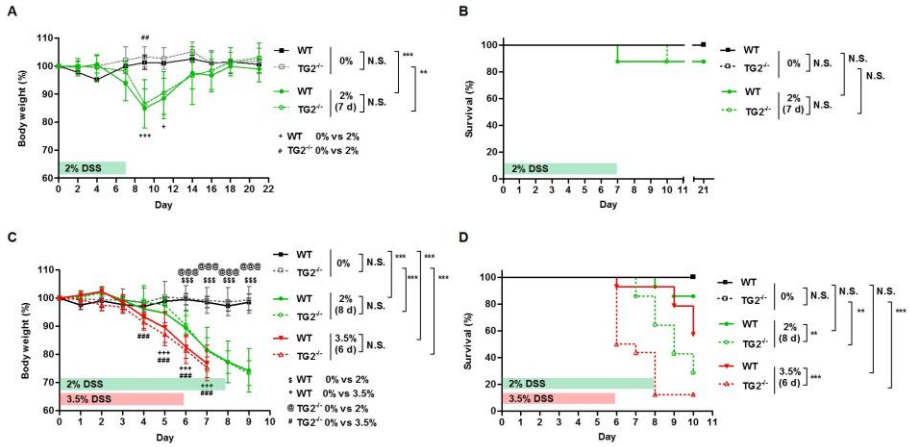

Figure 2. Body weight changes and survival rate in TG2$^{+/+}$ and TG2$^{-/-}$ mice during DSS treatment. (A, B) 14-week-old female TG2$^{+/+}$ and TG2$^{-/-}$ mice were fed *ad libitum* water containing 0 (n=2) and 2% (n=8) DSS for 7 days. (C, D) Age- and sex-matched TG2$^{+/+}$ and TG2$^{-/-}$ mice were fed *ad libitum* water containing 2 (n=14), and 3.5% (n=15) DSS for 8 and 6 days, respectively or plain water (n=6). (A, C) Body weight, expressed as percentage of weight on the day of first exposure to DSS, is plotted against time. The figure shows the mean values and standard deviations. Overall *P* values analyzed using two-way ANOVA are shown at the right; individual Bonferroni post-test results are shown above the line profiles. (B, D) Survival curves of TG2$^{+/+}$ and TG2$^{-/-}$ mice are depicted against time. The *P* values were calculated using Log-rank test. **P*<0.05; ***P*<0.01; ****P*<0.001. N.S; not significant.

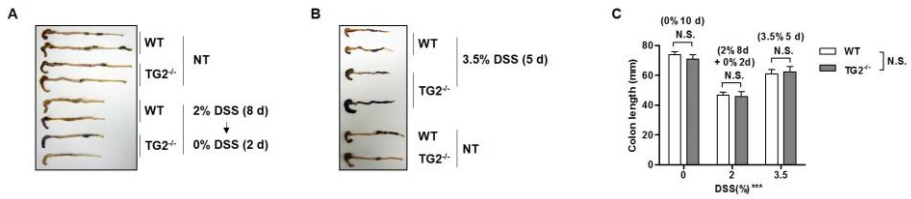

Figure 3. Colon length changes in TG2$^{+/+}$ and TG2$^{-/-}$ mice during DSS treatment. (A) Age- and sex-matched TG2$^{+/+}$ and TG2$^{-/-}$ mice were treated with plain (n=2) or 2%

DSS-water (n=4) for 8 days. After the mice were fed with plain drinking water for additional 2 days, they were euthanized and their colons were dissected. The representative two colons per group were took a picture. (B) The mice were administrated with plain (n=2) or 3.5% DSS-water (n=2) for 5 days. Their colons were separated and the representative two colons per group were photographed. (C) Length of colon removed from euthanized mice in A and B was measured and graphed as the mean values and standard deviations in each group. Overall *P* values analyzed using two-way ANOVA are shown at the right for mouse groups and the bottom for DSS doses; individual Bonferroni post-test results are shown above the columns. ***$P<0.001$. N.S; not significant.

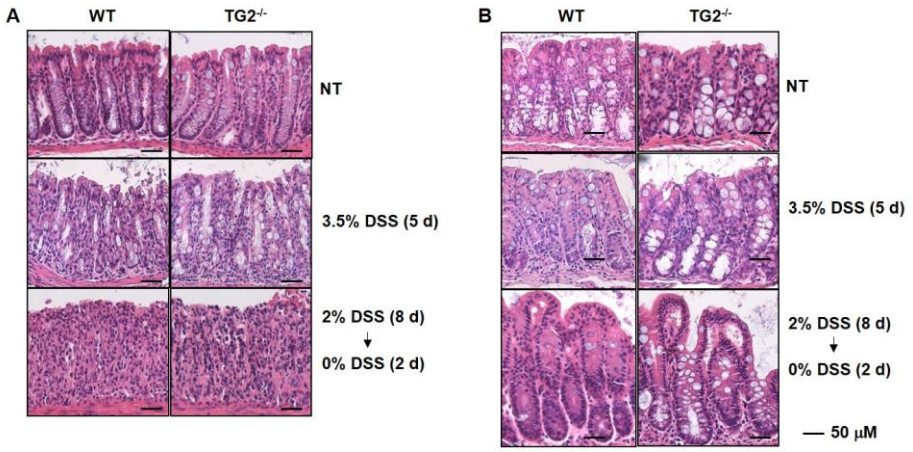

Figure 4. Histopathology of TG2$^{+/+}$ and TG2$^{-/-}$ mice treated with DSS. Age- and sex-matched TG2$^{+/+}$ and TG2$^{-/-}$ mice were administrated with plain or 3.5% DSS-water for 5 days or 2% DSS-water for 8 days and plain drinking water for additional 2 days. Colon sections were stained with hematoxylin and eosin. (A) Distal colon. (B) Proximal colon.

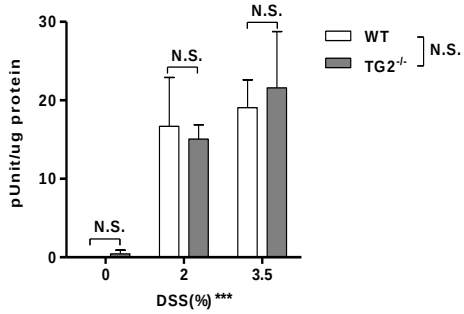

Figure 5. Myeloperoxidase (MPO) enzymatic activity in colon lesions of TG2$^{+/+}$ and TG2$^{-/-}$ mice treated with DSS. Age- and sex-matched TG2$^{+/+}$ and TG2$^{-/-}$ mice were administrated with plain (n=5) or 3.5% DSS-water (n=3) for 5 days or 2% DSS-water (n=3) for 7 days and plain drinking water for additional 3 days. MPO activity was measured in distal colons from TG2$^{+/+}$ and TG2$^{-/-}$ mice administered DSS-water as described in Materials and Methods. The activity was graphed as the mean values and standard deviations in each group. Overall *P* values analyzed using two-way ANOVA are shown at the right for each mouse group and the bottom for DSS doses; individual Bonferroni post-test results are shown above the columns. ****P*<0.001. N.S; not significant.

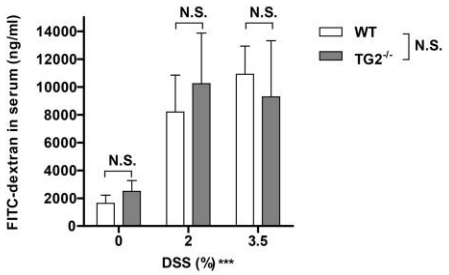

Figure 6. ***In vivo*** intestinal permeability test in **TG2$^{+/+}$** and **TG2$^{-/-}$** mice fed DSS. Age- and sex-matched TG2$^{+/+}$ and TG2$^{-/-}$ mice were administrated with plain (n=6) or 3.5% DSS-water (n=3) for 5 days or 2% DSS-water (n=3) for 7 days and plain drinking water for additional 3 days. TG2$^{+/+}$ and TG2$^{-/-}$ mice treated with DSS were gavaged with 60 mg/100 g body weight of FITC-dextran as described in Materials and Methods. Serum FITC-dextran level was quantified as a measure of intestinal permeability and graphed as the mean values and standard deviations in each group. Overall *P* values analyzed using two-way ANOVA are shown at the right for each

mouse group and the bottom for DSS doses; individual Bonferroni post-test results are shown above the columns. ***P<0.001. N.S; not significant.

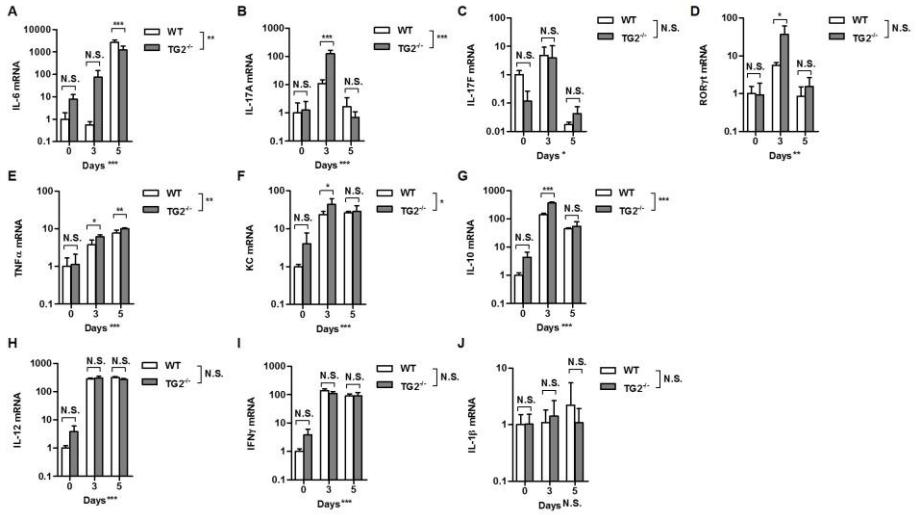

Figure 7. Comparison of expression levels of inflammatory mediators in colon between DSS-treated wild-type and TG2$^{-/-}$ mice. (A–I) Wild-type and TG2$^{-/-}$ mice were treated with 3.5% DSS-water for 3 or 5 days. Total RNA was prepared from distal colon and reverse transcribed. Using real-time PCR, relative mRNA levels of IL-6 (A), IL-17A (B), IL-17F (C), RORγt (D), TNFα (E), KC (F), IL-10 (G), IL-12 (H), IFNγ (I), and IL-1β (J) were determined and graphed as the mean values and standard deviations for each group. Overall P values analyzed by using two-way ANOVA are shown; individual Bonferroni post-test results are shown above the columns (n = 3 for each group). *P < 0.05; **P < 0.01; ***P < 0.001. NS, not significant.

4. Discussion

TG2 has been reported to importantly participate in the pathogenesis of various inflammatory diseases including lung fibrosis, cystic fibrosis, multiple sclerosis and sepsis (1). However, the role of TG2 in IBD has been remained elusive. In current study, we applied $TG2^{-/-}$ mice to DSS-induced acute colitis model to explore TG2 roles in pathogenesis of IBD. $TG2^{-/-}$ mice showed the distinct expression profiles of some colonic inflammatory mediators and higher lethality under severe colitis conditions when compared with $TG2^{+/+}$ mice. However, there were no significant differences between $TG2^{+/+}$ and $TG2^{-/-}$ mice groups in well-established clinical and histological parameters including body weight loss, colon shortening, histological changes, MPO activity, and *in vivo* intestinal permeability. These results indicate that TG2 does not play critical roles in DSS-induced acute colitis.

DSS is directly toxic for epithelial cells in large intestinal basal crypts, leading to disruption of mucosa barrier integrity (21). In this model, colitis is generally considered to be initiated by this injury which induce the increasing of intestinal mucosal permeability for enteric commensal bacteria. TG2 is known to be activated by tissue injuries disrupting integrity of extracellular membrane components or plasma membrane (4). Under normal condition, TG2 was expressed but inactive in mouse colon (Fig. 1), supporting that TG2 is expressed as a latent form but is activated under stressed conditions (3, 4). Meanwhile, TG2 protein levels were increased and its activity was appeared in whole colon sections of $TG2^{+/+}$ mice but not of $TG2^{-/-}$ mice by DSS administration (Fig. 1). These data indicate that TG2 is a sole isozyme for TG activity in mouse colon inflamed by treatment of DSS. Interestingly, TG2 was expressed at low levels but highly activated in CA cells of DSS-treated mouse colon (Fig. 1). It is likely that TG2 activity was triggered by physically destructive damage of CA cells through direct exposure to DSS (21).

Notwithstanding the activation of colonic TG2 by DSS administration, TG2 was not involved in DSS-induced colitis. It implies that TG2 activation might be a consequence not a cause of colitis in this model. This result corresponds

with role of TG2 in poly(I:C)-induced enteropathy mouse model in which TG2 activity was observed at villus tips but not relevant to villous atrophy in small intestine of poly(I:C)-treated mice (25). Taken together, TG2 activity seems to be just one of the cellular responses to intestinal injury or inflammatory cues without being involved in the severity of enteropathy. However, interestingly, TG2 is proposed to be associated with exacerbation of small intestine damage caused by administration of dietary gliadin in poly(I:C)-treated gliadin-sensitive NOD-DQ8 mice (26). Thus, it is plausible that DSS-mediated enteropathy might be aggravated by intestinal TG2 activity only under the additional conditions like to mimic celiac disease. These results suggest that TG2 activity may be responsible for an initial inflammatory response in intestine just through modification of gliadin peptide and thereby generation new epitope but not through modulation of cellular inflammatory signaling itself.

TG2 has been reported to increase the expression levels of pro-inflammatory cytokines including IL-6, TNFα, IFNγ, IL-17A and IL-17F in the process of LPS or TNFα/Actinomycin D-induced sepsis (13, 27) or bleomycin-induced lung fibrosis (9) through the activation of NF-κB signaling pathway. The expression levels of these cytokines in colon tissues are all crucially correlated with the severity of the DSS-triggered colitis (28). In this study, IL-6 significantly decreased in colon samples of $TG2^{-/-}$ mice 5 day after DSS treatment as compared to corresponding $TG2^{+/+}$ mice (Fig. 7A). In contrast, the expression levels of IL-1β, IL-12, IL-17F and IFNγ were unaffected by TG2 in DSS-treated mice colons (Figs. 14F-14I). These results indicate that TG2 may specifically up-regulate the expression levels of IL-6 which is mainly generated in bone marrow-derived cells (29) and play a pro-inflammatory and regenerative role in DSS-induced mouse colitis (30, 31) as well as human IBD (32). In this study, however, the reduced extent of colonic IL-6 levels in $TG2^{-/-}$ mice did not influenced on the severity of DSS-induced colitis.

DSS induces the expression of IFNγ in colon tissue which is a cytokine produced during Th1 cell response (28). Recently, IFNγ has been reported to be

able to activate intestinal TG2 through extracellular and intracellular signaling pathway (33, 34). Extracellular oxidized TG2 was suggested to be reduced and activated by thioredoxin that is secreted from monocytes triggered by IFNγ at small intestinal tissue (33). On the other hand, IFNγ was reported to induce TG2 expression level via intracellular phosphoinositide 3-kinase pathway in T84 colorectal carcinoma cells (34). Thus, IFNγ might be related with colonic TG2 activation in mouse dosed with DSS (Fig. 1), but it needs to be verified in the future. Meanwhile, since IFNγ can be produced from Th1 cells reactive to dietary gluten deamidated by TG2, it has been proposed that there is a positive loop for auto-amplification between TG2 activity and IFNγ in the celiac intestine (34). However, TG2 was not involved in the regulation of IFNγ expression in colon tissue of C57BL/6 mice administrated with DSS under gluten-free chow diet (Fig. 7H). It implies that TG2 is not a general modulator for Th1 cell response.

The expression levels of KC, IL-17A, and IL-10 on 3 day and TNFα on 3 and 5 days after DSS administration were rather up-regulated in $TG2^{-/-}$ mice colon compared with $TG2^{+/+}$ mice colon (Fig. 7). KC is a chemokine expressed by macrophages and neutrophils and promotes the neutrophil to infiltrate into tissue lesion via a C-X-C chemokine receptor type 2 (CXCR2) signal pathway. CXCR2 ablation reduced and recombinant KC administration exacerbated DSS colitis (35). However, there were no difference in the number of infiltrated neutrophils and MPO activity between $TG2^{+/+}$ and $TG2^{-/-}$ mice colons (Fig. 4 and 5), suggesting that the increased levels of colonic KC in $TG2^{-/-}$ mice were not critical to change the colitis phenotype.

TNFα has been emerged as pro-inflammatory cytokines in various diseases. Recently, however, TNFα has been reported to suppress DSS colitis by promoting glucocorticoid synthesis in the injured colon (36). Moreover, IL-10 has been known to critically work as a suppressive cytokine for colitis in mouse (37, 38) and human (39, 40). However, in this study, the higher levels of these anti-colitogenic cytokines in colon of DSS-dosed $TG2^{-/-}$ mice than those of the corresponding $TG2^{+/+}$ mice were not affected to colitis severity.

Lately, we showed that TG2 increased the expression levels of IL-6 in lung epithelial cells, leading to differentiate naïve T cells to Th17 cells and raise the secretion levels of IL-17A in bleomycin-induced lung fibrosis (9). In contrast, DSS-induced intestinal expression levels of IL-17A and RORγt were enhanced by TG2 ablation (Fig. 7E) even though the expression of colonic IL-6 was positively regulated by TG2 (Fig. 7A). These results suggest that TG2 down-regulates the Th17 pathway in DSS-induced acute colitis model. Intriguingly, IL-17A has been thought to play a protective role in gastrointestinal track through induction of the expression levels of mucosal barrier integrity regulating genes, including claudins which are important proteins to form the tight junctions between intestinal epithelial cells (41). Indeed, IL-17A ablation led to aggravate DSS-induced colitis (42, 43) and T cell transfer-induced colitis (44) in mice. Besides, secukinumab, an IL-17A-specific blocking antibody has been reported to exacerbate CD (45). Since TG2 is known to be involved in regulation of cell adhesion and ECM integrity (1), it is plausible that TG2-ablation-medited loss of integrity of the intestinal epithelial barrier boosts the Th17 pathway in DSS-induced colitis in $TG2^{-/-}$ mice, favoring the homeostasis of immune response to enteric commensal bacteria. However, we did not find any clue about TG2 involvement in maintaining intestinal epithelial cell integrity.

$TG2^{-/-}$ mice have revealed increased survival rates compared to $TG2^{+/+}$ mice in LPS-induced sepsis (13, 27). It is thought to be due to the reduction of NF-κB-dependent cytokine production in TG2-absent macrophages triggered by LPS, leading to reduction of tissue damages such as liver (13, 27). In contrast, TG2 worked as a survival factor in DSS-induced colitis, even though TG2 was not relevant to DSS-induced colitis pathogenesis (Figs. 2B and 2D). This is consonant with TG2 role in TNFα/Actinomycin D-induced sepsis (27), carbon tetrachloride-induced liver injury (46), and poly(I:C)-induced enteropathy (25). In carbon tetrachloride-induced liver injury and TNFα/Actinomycin D-induced sepsis, TG2 was suggested to protect liver from tissue damage rather than to induce inflammatory responses in macrophages (27, 46). In this view, since there was no significant phenotypic difference between $TG2^{+/+}$ and $TG2^{-/-}$ mice

in DSS-induced colitis as well as poly(I:C)-induced enteropathy (25), these chemical-induced mouse survival rate might be affected by protective effects of TG2 in other tissues such as liver rather than its intestinal inflammatory effects. DSS is known to be not degraded but penetrate epithelial cell layer in intestine (47). Absorbed DSS is thought to be eliminated by phagocytosis of majorly Kupffer cells in the liver and auxiliary macrophages in the spleen (48). The absence of TG2 revealed the reduced capacity of phagocytic uptake of apoptotic cells in macrophages (49) and low level of $gp91^{phox}$ subunit of the phagocytic NADPH oxidase to destroy invaded bacteria, cell debris, and foreign materials in neutrophils (50). Thus, it is possible that DSS could not be efficiently removed but accumulated in liver or spleen in TG2-deficient mice, resulting in induction of liver or spleen tissue damage and increase of lethality to DSS. Similarly, in the case of poly(I:C)-induced enteropathy, the increase of lethality to poly(I:C) of TG2-null mice could be due to malfunction of other organs rather than intestine itself (25) since intraperitoneally administrated poly(I:C) can be distributed systemically and induce injury response in various organs such as liver (51) and brain (52).

This study show that intestinal TG2 activity was not associated with DSS-induced acute colitis. However, the enzymatic activity is thought to essentially participate in the pathogenesis of celiac disease, producing autoantibody for TG2 in the process of gluten peptide deamidation (7). Intriguingly, anti-TG2 antibody was also detected in serum of patients suffering from UC as well as CD (20). It is thus wondered whether dietary gluten peptide or other food peptides could be an immunotoxic substrate of TG2 in DSS-treated mice or IBD patients, intensifying the enteropathies. This all information will be helpful to understand the exact pathological role of TG2 and develop more effective therapeutic drugs in IBD including celiac disease.

CHAPTER 2

Dexamethasone downregulates caveolin-1 causing muscle atrophy via inhibited insulin signaling

1. Introduction

Muscle atrophy is the loss of muscle mass that leads to muscle weakness, occurring with various conditions and diseases, including cancer, severe injury, sepsis, steroid therapy and aging (53-56). Recently, glucocorticoid is widely used for many medical conditions, thus steroid-induced muscle atrophy become a serious problem because muscle wasting aggravates underlying diseases and increases mortality, especially in aged patients (53). At present, however, there is no effective method to prevent the muscle atrophy in steroid therapy.

Glucocorticoid binds to the specific receptor which translocates into nucleus and modulates various cellular processes by regulating the transcription of a number of genes (57-59). In muscle, glucocorticoid treatment promotes degradation of muscle proteins and also suppresses synthesis of muscle protein by increasing the expression of two muscle-specific ubiquitin ligases, MuRF1 and MAFbx/Atrogin-1 (60). MuRF1 ubiquitinylates and degrades troponin I, myosin heavy chain and myosin binding protein C through proteasomal system (61-63). In contrast, increase of MAFbx/Atrogin-1 leads to suppression of protein synthesis through ubiquitinylation and degradation of eIF3f and MyoD, key factors for translation and transcription in muscle, respectively (64). Recently, it was reported that glucocorticoid regulates MuRF1 and MAFbx/Atrogin-1 by targeting two genes, REDD1 and KLF15. REDD1 inhibits mTOR by stabilizing the TSC1-TSC2 complex, thereby suppressing protein synthesis in muscle (65) and KLF15 increases expression of FoxO, a transcription factor for promoting MAFbx/Atrogin-1 and MuRF1 expression (66). These findings indicate that crosstalk between glucocorticoid and IGF1 signaling pathway play a crucial role in coordinating protein synthesis and degradation.

Caveolin (Cav) is the major protein component of caveolae which are invaginations of plasma membrane found in most cell types (67). Cav functions as a scaffolding protein within caveolae, and is involved in the regulation of signaling pathways through interaction with a number of membrane proteins such as G-proteins or receptors. In muscle, three Cav isoforms are known to be

expressed (68). Cav3 is expressed predominantly in muscle forming homo-oligomer in T tubule system, plays a role in muscle development and sarcolemma repair under mechanical-stressed conditions (69). Mutations in the Cav3 gene cause several degenerative muscle diseases in human, including limb-girdle muscular dystrophy, ripping muscle disease and distal myopathy. Cav1 is also expressed in muscle and lung, and forms homo-oligomer or hetero-oligomer with Cav2 (70). Cav1-deficient mice show impaired nitric oxide and calcium signaling resulting in dilated cardiomyopathy and thickening of alveolar septa in the lung (71),(72). In human, mutations in the Cav1 gene cause generalized lipodystrophy, insulin resistance and hypertriglyceridemia (73).

Previously, we have demonstrated that Cav1 in skeletal muscle is related to insulin sensitivity *in vitro* and *in vivo* (74). Cav1 expression in skeletal muscle increases with development, whereas its expression decreases after aging (75). Additionally, Cav1-disrupted mice show lean body mass, suggesting a role for Cav1 in the maintenance of muscle mass (76). Moreover, Cav1 status in skeletal muscle tissues is dependent on exercise and sex steroid status (77, 78). These results and phenotypes of Cav-deficient mice suggest that Cavs may be involved in the regulation of skeletal muscle mass under metabolically stressed conditions.

In this study, we therefore evaluate the role of Cav isoforms in a glucocorticoid-induced muscle atrophy model, and found that dexamethasone (DEX) treatment decreases Cav1, but not Cav2 and Cav3 expression. Down-regulation of Cav1 suppresses the expression of insulin receptor and insulin receptor substrate-1, resulting in an increase of MAFbx/Atrogin-1 and MuRF-1. Conversely, overexpression of Cav1 prevents DEX-induced muscle atrophy *in vitro* and *in vivo*. Our results indicate that Cav1 mediates glucocorticoid-induced suppression of insulin signaling.

2. Materials and Methods

2-1. Cell culture

C2C12 cells (American Type Culture Collection) were cultured in Dulbecco's modified Eagle's Medium (DMEM) supplemented with 10% fetal bovine serum (FBS), 100 U/mL penicillin, and 100 μg/mL streptomycin. To induce myoblast fusion and differentiation, cells were grown to about 80% confluency, and the medium was replaced with DMEM containing 2% FBS. The medium was changed every 2 days. After 4 days, the C2C12 myotubes were treated with various doses of DEX (100 nM, 1 μM, 10 μM, and 100 μM) for indicated time to induce myotube atrophy.

2-2. Measurement of myotube diameter

After differentiation, C2C12 myotubes were stained with a modified PAS staining kit (Merck, Whitehouse Station, NJ, USA). The cells were treated for 5 min with periodic acid, followed by washing with PBS for 3 min. Then, Schiff's reagent was added to the cells for 15 min at room temperature. After washing with PBS, nuclei were stained for 2 min with Gill III solution. The cells were mounted in Neo-Mount solution and photographed under a phase contrast microscope at 100× magnification. The diameters of 50 myotubes were measured at least in ten random fields using the ImageJ software (NIH, Frederick, MD, USA). The results are expressed as a percentage of the diameter of the controls.

2.3 Transfection and luciferase assays

C2C12 cells (2×10^4) were seeded into each well of 12-well plates and cultured for 24 h. Cells were then transfected with the reporter constructs using Lipofectamine 2000 (Invitrogen) according to the manufacturer's instructions. When the cells reached confluence, cells were cultured in differentiation medium for 4 days, and then treated with 1 μM of DEX for 24 h. After preparing cell lysates, luciferase activity was assayed using a dual luciferase reporter assay system (Promega, Madison, WI, USA) and normalized by *Renilla*

luciferase activity. The results are expressed as means ± SD of at least five independent experiments.

2-4. Western blot analysis

C2C12 myotubes were lysed with RIPA buffer (10 mM Tris-HCl, pH 7.5, 1 mM EDTA, 150 mM NaCl, 1% Triton X-100, 1 mM protease inhibitor cocktail (Roche, Indianapolis, IN, USA), 1 mM PMSF, 50 mM sodium fluoride, and 0.2 mM sodium vanadate). Lysates were boiled in sample buffer (50 mM Tris-HCl, pH 6.8, 2% SDS, 0.14 M 2-mercaptoethanol, 10% glycerol, and 0.001% bromophenol blue). Samples were resolved by SDS polyacrylamide gel electrophoresis, transferred to nitrocellulose membranes, and blocked with Tris-buffered saline containing Tween-20 in 5% nonfat dry milk. The membranes were incubated with primary antibodies overnight at 4°C. We used the following primary antibodies: MAFbx/Atrogin-1 (ECM Bioscience, Versailles, KY, USA), MuRF1 (GeneTax, Irvine, CA, USA), caveolin-1, -2, -3 (BD, Franklin Lakes, NJ, USA), MyoD (Santa Cruz Biotechnology), EIF3F (Abcam, Cambridge, MA, USA), p-GR (Cell Signaling Technology, Danvers, MA, USA), α-tubulin (Sigma, St. Louis, MO, USA), insulin receptor α (IRα, Santa Cruz Biotechnology), and insulin receptor substrate-1 (IRS-1, Cell Signaling Technology). Secondary antibodies were added for 1 h at room temperature. The antibody-antigen complexes were detected using an enhanced chemiluminescence kit (Pierce, Rockford, IL, USA). The signal intensity was determined using an LAS-3000 image reader (Fujifilm, Tokyo, Japan).

2-5. Real-time quantitative RT-PCR

Total RNA was isolated from C2C12 cells using the TRI reagent (Invitrogen, Grand Island, NY, USA), and the expression levels of MAFbx/Atrogin-1, MuRF1, caveolin-1, and GAPDH mRNA was assessed by real-time RT-PCR using an iCycler RT-PCR instrument (Bio-Rad, Hercules, CA, USA). For each sample, 25 ng of total RNA were subjected to RT-PCR (in duplicate) according to the protocol provided by the manufacturer. The following specific primers were used: MAFbx/Atrogin-1, 5′-CTCTGTACCATGCCGTTCCT-3′ (forward)

and 5′-GGCTGCTGAACAGATTCTCC-3′ (reverse); MuRF1, 5′-TGTCTG GAGGTCGTTTCC G-3′ (forward) and 5′-TGCCGGTCCATGATCACTT-3′ (reverse); caveolin-1, 5′-ACG ATGTCTGGGGGCAAATAC-3′ (forward) and 5′-TCATATCTCTTTCTGCGTGC-3′ (reverse); and GAPDH, 5′-CCACCC ATGGCAAATTCCATGGCA-3′ (forward) and 5′-TCTAGACGGCAGGTC AGGTCCACC-3′ (reverse).

2-6. siRNA knockdown of caveolin-1

siRNA specific for Cav1 was purchased from Santa Cruz Biotechnology (Santa Cruz, CA, USA). siRNA (10 nM) was transfected into C2C12 cells for 10 min using the G-Fectin transfection protocol (Genolution Pharmaceuticals, Seoul, Korea).

2-7. Promoter analysis

Cav1 promoter region (GenBank accession number NC_000072.6) flanking from -2000 to +300 was amplified from genomic DNA using PCR (Roche Molecular Biochemicals, Indianapolis, IN, USA). Four deletion mutants of Cav1 promoter, flanking from -2000, -1037, -500 and -100 to +300, were generated using PCR and cloned into pGL2-Basic (Promega , Madison, WI, USA) for the luciferase assays. Site-directed mutagenesis was performed following the manufacture's instruction (Stratagene, La Jolla, CA, USA). All constructs were verified by DNA sequencing (Applied Biosystems 3730xl DNA Analyzer). To define the transcriptional upstream region of Cav1 gene, we used the FASTA data from the NCBI (http://www.ncbi.nlm.nih.gov/nuccore/NC_000072.5). Putative GRE sequences were identified in the region (-2000 to +300) of Cav1 gene using http://www.cbil.upenn.edu/cgibin, http://alggen.lsi.upc.es/cgibin/promo_v3 and http://www.gene-regulation.com/cgi-bin.

2-8. Animals

Male C57BL/6 mice (8 months old) were purchased from the Osong Aging Animal Laboratory (Chungcheong bukdo, Korea). Mice were given *ad libitum*

access to food and water, and were maintained in a 12/12-h light/dark cycle. All animal procedures were approved by the Institutional Animal Care and Use Committee at the Seoul National University College of Medicine. Animals were randomly assigned to four groups (n = 5 for each group): control group received saline, DEX group received 5 mg/kg of DEX by every other day i.p. injection for 12 days, DEX-AdGFP group received adenovirus expressing GFP by daily injection to gastrocnemius muscle in eight places for 3 days after DEX treatment and DEX-AdCav1 group received adenovirus expressing Cav1 by daily injection to gastrocnemius muscle in eight places for 3 days after DEX treatment.

2-9. Preparation of adenovirus

The adenoviral vectors and infective recombinant adenovirus expressing Cav1 used in this study were described previously (74). In brief, infective recombinant adenovirus was made using the AdEasy system. Cav1 cDNA was inserted into pAdTRACK-CMV plasmid (Invitrogen, Carlsbad, CA, USA) and performing homologous recombination in E.coli BJ5183 with this vector and a large adenovirus containing pAdEasy-1 plasmid following electroporation. Recombinant viruses were selected with kanamycin. Virus stocks amplified in HEK293 cells on 15cm plates and purified using kits (BD Adeno-X Purification kits; Clontech, Palo Alto, CA, USA).

2-10. Measurement of muscle fiber cross-sectional area

Muscle sections (10 μm) were obtained and mounted on glass slides. The sections were fixed for 2 min with acetone and stained with H&E. Images of muscle fiver cross-sectional area (CSA) were visualized at X200 magnification using light microscope and captured with a microscope camera (Zeiss, Oberkochen, Germany). At least 200 fibers per muscle were randomly chosen and analyzed using Image J software.

2-11. Statistical analysis

Results were expressed as mean ± SD. Differences between two variables were assessed by unpaired Student's *t* test. The difference was considered significant if the *p* value was <0.05. All statistical calculations were performed using Prism 5.0 (GraphPad Software, San Diego, CA).

3. Results

3-1. Dexamethasone negatively regulates caveolin-1 expression

To examine the role of caveolins (Cavs) in glucocorticoid-induced muscle atrophy, we used dexamethasone (DEX)-treated C2C12 cells as an *in vitro* model (79-82). C2C12 myotubes were treated with DEX at several concentrations (100 nM, 1 μM, 10 μM, and 100 μM) for various period of time. Western blot analyses showed that DEX treatment induces maximum expression of glucocorticoid receptor (GR) even at 100 nM (Fig. 1A) and translocation of GR into nucleus (Fig. 1B). The levels of MAFbx/Atrogin-1 and MuRF1, muscle atrophy markers, were increased in a dose- and time-dependent manner, peaked at 1 μM for 24 hr of DEX-treatment, which was confirmed by real-time RT-PCR (Fig. 1A and 1C). In contrast, the levels of muscle differentiation markers, MyoD and EIF3F, and the insulin signaling molecules IRα and IRS-1 were decreased in a dose- and time-dependent manner by DEX-treatment (Fig. 1A). These effects of DEX resulted in a 20% reduction of the mean diameters of myotubes after 1 μM of DEX- treatment for 24 h, compared with the control (Fig. 1D).

Under the same experimental conditions, we found that the level of Cav1 decreased in a dose-dependent manner while the levels of Cav2 and Cav3 did not change in DEX-treated C2C12 myotubes (Fig. 1A). DEX regulates the transcription of a number of genes in a positive or negative way. To test whether DEX regulates Cav1 expression at transcriptional level, we performed real-time RT-PCR and found that Cav1 mRNA significantly decreased in cells treated with DEX (Fig. 1E). Moreover, we observed that MG132 showed no effect on the Cav1 protein level after DEX treatment (data not shown), indicating that Cav1 is down-regulated by DEX through transcriptional suppression, but not through atrogin1 or MuRF1-mediated proteolytic degradation.

To further confirm the transcriptional regulation of Cav1 by DEX, we generated the promoter deletion constructs based on the sequence analysis that shows about 30 putative glucocorticoid-responsive elements (GREs) within 2 kbp upstream of the transcription start site of Cav1 gene. The deletion

constructs fused with a luciferase reporter were transfected into the C2C12 cells. Reporter assay revealed that DEX caused a 50% reduction in luciferase activity compared with controls, but failed to exhibit suppressive effect by deletion of the region spanning from -500 to -100 of the Cav1 gene (Fig. 2A). To determine specific GRE responsible for negative regulation of Cav1 gene, we generated six GRE mutants located in this region and found that the site-specific mutation (cagag to cacag) of GRE located at -387 failed to respond to DEX (Fig. 2B and Fig. 6). These results indicate that DEX suppresses Cav1 expression in C2C12 cells through negative regulatory GRE.

3-2. Caveolin-1 mediates DEX-induced suppression of insulin signaling

Cav1 plays a role as a scaffolding protein that recruits components of various signaling pathways to caveolar membrane, thereby activating or repressing signaling (83). To test whether Cav1 is involved in the regulation of signaling pathways for muscle growth or protein degradation, we first examined the effect of Cav1-knockdown on insulin signaling. C2C12 cells were treated with Cav1-specific siRNA for 24 h, and protein levels of IRα and IRS-1 were evaluated. Cav1 siRNA treatment resulted in a 40% reduction in Cav1 protein compared with control siRNA-treated cells. In these cells, protein levels of IRα and IRS-1 were significantly decreased up to 90% and 80%, respectively, compared with the levels of control siRNA-treated cells (Fig. 3A and 3B). Since the reduced insulin signaling results in decreased activity of Akt which leads to a marked increase of nuclear FoxO, promoting E3 ligase expression (84), we next examined the protein level of E3 ligases in Cav1 siRNA-treated cells. Western blot analyses showed that protein levels of MAFbx/Atrogin-1 and MuRF1 were significantly increased up to 3- and 10-folds, respectively (Fig. 3A and 3B). Moreover, we observed that Cav1-knockdown caused a 20% reduction in diameters of myotubes, compared with control siRNA-treated cells (Fig. 3C and 3D). These results indicate that Cav1 mediates DEX-induced suppression of insulin signaling, resulting in an increase of E3 ligases expression.

To confirm the causal relationship between Cav1 expression and insulin

signaling, we tested whether Cav1-overexpression could suppress E3 ligases expression through upregulation of insulin signaling. To this end, adenovirus expressing Cav1 (AdCav1) was generated and infected to cultured C2C12 cells. Western blot analysis showed that the protein level of Cav1 increased by 1.7-fold compared with control virus-infected cells. Under the same experimental conditions, the levels of IRα and IRS-1 were elevated by 3-fold and 2-fold, respectively. Concomitantly, protein levels of MAFbx/Atrogin-1 or MuRF1 were decreased by 30% and 70%, respectively (Fig. 4A and 4B). Moreover, when these cells were treated with DEX, Cav1-overexpression prevented more than 80% of the DEX-induced reduction in IRα and IRS-1expression, and 25% - 60% of the DEX-induced increase in MAFbx/Atrogin-1 and MuRF1expression (Fig. 4A and 4B). In addition, when the diameters of myotubes were compared, Cav1-overexpression prevented up to 20% of DEX-induced reduction of mean diameters (Fig. 4C and 4D). These results obtained from siRNA and adenoviral overexpression systems indicate that Cav1 plays a role as a key mediator in the regulation of DEX-induced insulin signaling.

3-3. Caveolin-1 overexpression restores muscle loss in DEX-treated mice

We next sought to extend these results from cellular model to an *in vivo* model of DEX-induced muscle atrophy by assessing whether Cav1 overexpression could restore the muscle loss induced by DEX-treatment. C57BL/6 mice were injected intraperitoneally with DEX (5 mg/kg of body weight) every other day for 12 days, and then treated with daily injection of AdCav1 or AdGFP virus to gastrocnemius muscle in eight places for 3 days.

DEX-treatment and adenovirus injection had no significant effect on the body weight of mice over the duration of the treatment period (Fig. 7A), but AdCav1 injection restored the weight loss of gastrocnemius muscle induced by DEX-treatment (Fig. 7B), which was confirmed by the increased ratio of gastrocnemius /body weight (Fig. 7C). Moreover, when assessed the levels of proteins, Cav1 overexpression by AdCav1 injection reversed the DEX-induced decrease of IRα and IRS-1, resulting in decrease of E3 ubiquitin ligases (MAFbx/Atrogin-1 and MuRF1), and increase of MyoD and EIF3F in

gastrocnemius muscle (Fig. 5A and 5B). By contrast, Cav1 overexpression had no effects on the expression of Cav2 or Cav3 (Fig. 5A).

To further confirm the restoring effect of Cav1 expression on DEX-induced muscle atrophy, the cross-sectional area (CSA) of myofibers in GA muscle was measured after H&E staining (Fig. 5C). In mice treated with DEX, the number of myofiber with larger CSA in gastrocnemius muscle was decreased compared with saline-treated mice. Injection with AdCav1 into gastrocnemius muscle of DEX-treated mice resulted in an increase of the number of myofiber with larger CSA compared with AdGFP virus-injected mice (Fig. 5D). These results indicated that Cav1 overexpression reversed DEX-induced muscle atrophy *in vivo*.

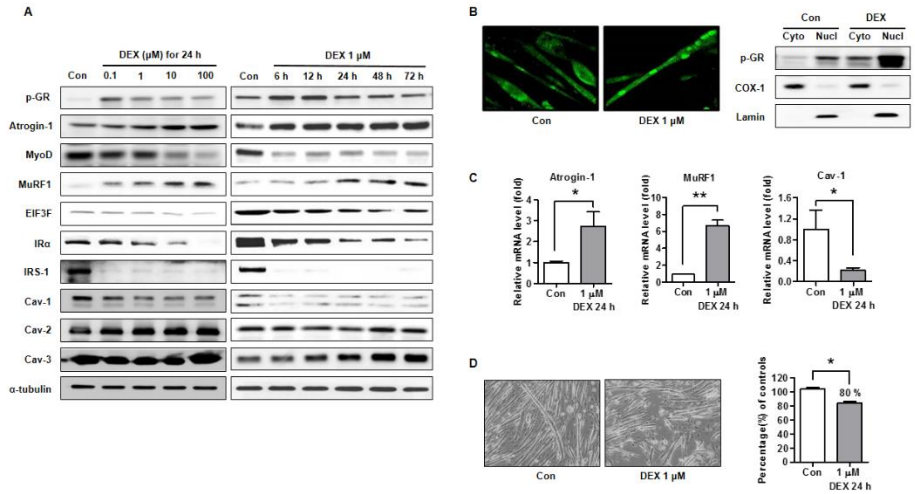

Figure 8. **Dexamethasone suppresses caveolin-1 expression at transcriptional level in C2C12 myotubes.** (A) Effect of dexamethasone treatment on the expression of caveolins. C2C12 cells were treated with dexamethasone (100 nM, 1 μM, 10 μM, and 100 μM) for various period of time. Cell lysates were analyzed by Western blotting using antibodies against phosphorylated glucocorticoid receptor (p-GR), MAFbx/Atrogin-1, MyoD, MuRF1, EIF3F, insulin receptor α (IRα), and IRS-1, caveolin-1 (Cav-1), caveolin-2 (Cav-2) and caveolin-3 (Cav-3). (B) Nuclear translocation of p-GR following dexamethasone treatment (1 μM, 2 h) was monitored by confocal microscopy and Western blot analysis. Cox-1 and lamin was used as

markers for the cytosolic (Cyto) and nuclear (Nucl) fractions, respectively. (C) Total RNA from C2C12 cells treated with 1 μM of dexamethasone for 24 h was analyzed by quantitative RT-PCR for MAFbx/Atrogin-1 and MuRF1 (n = 3). The data are given as mean ± SD. $^{**}P < 0.01$. (D) Myotubes treated with dexamethasone (1 μM, 24 h) were stained with PAS and photographed. Diameter of myotubes from randomly selected fields was measured using ImageJ program. The diameters are expressed as percentages of the control (n = 50). Results are expressed as mean ± SD. $^{*}P < 0.05$. (E) Effect of dexamethasone treatment (1 μM, 24 h) on Cav-1 mRNA expression analyzed by quantitative RT-PCR (n = 3). The data are given as mean ± SD. $^{**}P < 0.01$

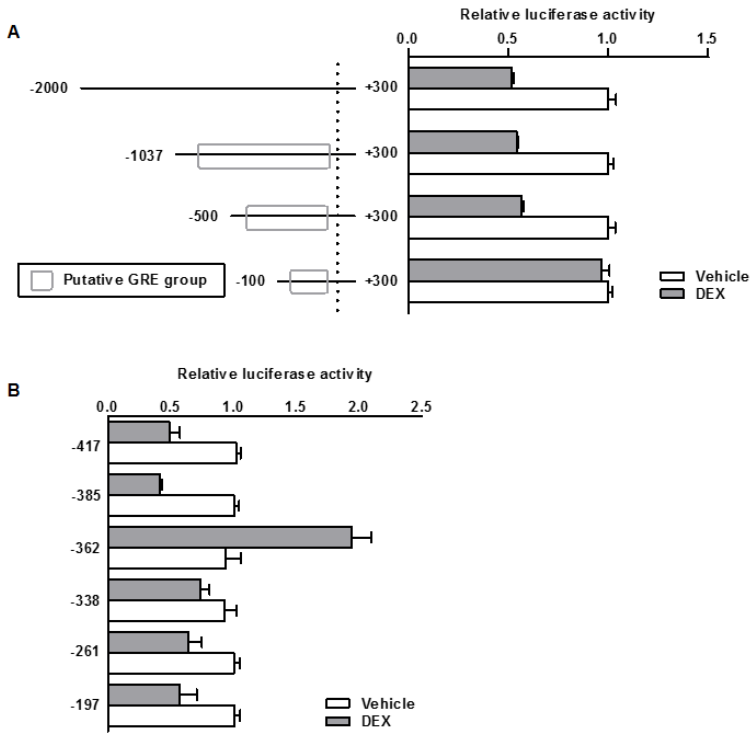

Figure 9. Identification of negative glucocorticoid-responsive element in mouse caveolin-1 promoter. (A) Luciferase reporter activity of deletion constructs for mouse caveolin-1 promoter. C2C12 cells transfected with deletion constructs were treated with 1 μM of dexamethasone for 24 h. Cell lysates were assayed for luciferase activity. (B) Effect of site-specific mutagenesis of GREs (cagag to cacag) on the reporter activity. Luciferase activity is expressed as a relative value to that of vehicle-treated cells (n = 5). Data represent mean ± SD.

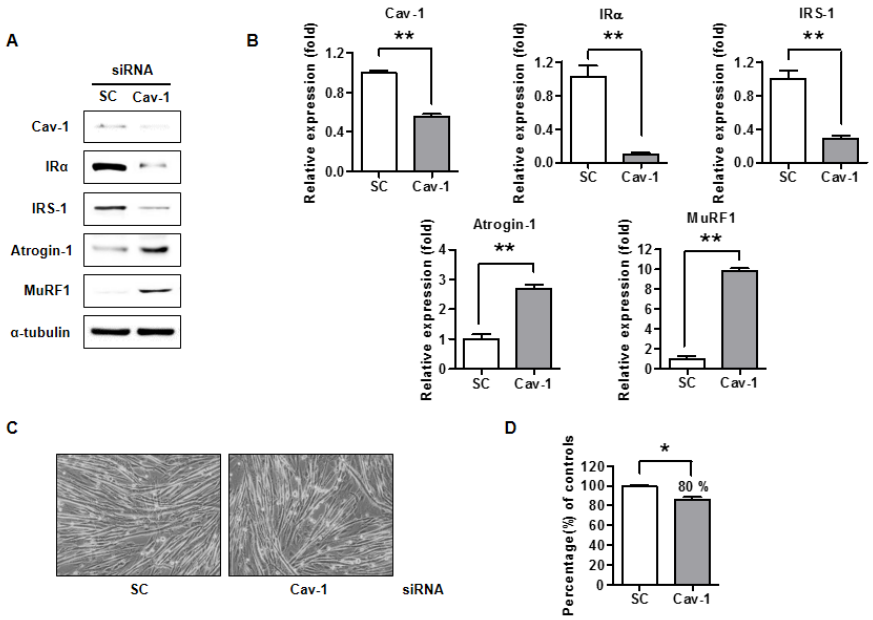

Figure 10. **Caveolin-1 knock-down induces a decrease of C2C12 myotube diameter through downregulation of IRα and IRS-1.** (A) Western blot analyses for C2C12 cells treated with caveolin-1 siRNA using antibodies against IRα, IRS-1, MAFbx/Atrogin-1 and MuRF1. (B) Relative band intensities of Western blot from three independent experiments were estimated by densitometric quantification. Data represent mean ± SD. $^{**}P < 0.01$. (C) Representative Photographs of C2C12 cells treated with caveolin-1 or scramble siRNA. (D) Cells were stained with PAS and photographed. The diameter of myotubes from randomly selected fields was measured using ImageJ program. Data are expressed as percentages of the control ($n = 50$). Results are given as mean ± SD. $^{*}P < 0.05$.

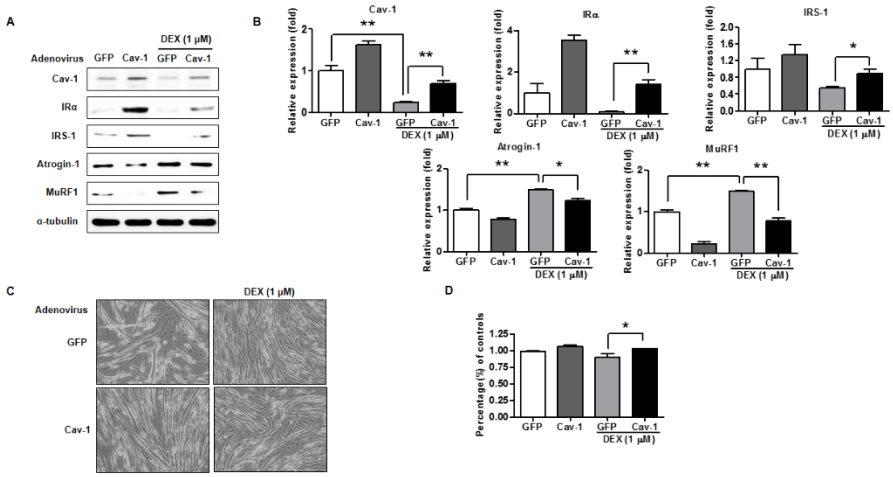

Figure 11. **Caveolin-1 overexpression prevents dexamethasone-induced decrease of myotube diameter.** (A) Western blot analysis for C2C12 myotubes infected with adenovirus expressing caveolin-1 (AdCav1, 3×10^{11} plaque-forming units) or green fluorescence protein (AdGFP, 3×10^{11} plaque-forming units) using indicated antibodies. Cells were cultured for 24 h in the presence or absence of dexamethasone (1 μM). (B) Relative band intensities of Western blot from three independent experiments were estimated by densitometric quantification. Data represent mean ± SD. $^{**}P < 0.01$; $^{*}P < 0.05$. (C) Representative Photographs of C2C12 cells infected with AdCav1 or AdGFP. (D) Cells were stained with PAS and photographed. The diameter of myotubes from randomly selected fields was measured using ImageJ program. Data are expressed as percentages of the control ($n = 50$). Results are given as mean ± SD. $^{*}P < 0.05$.

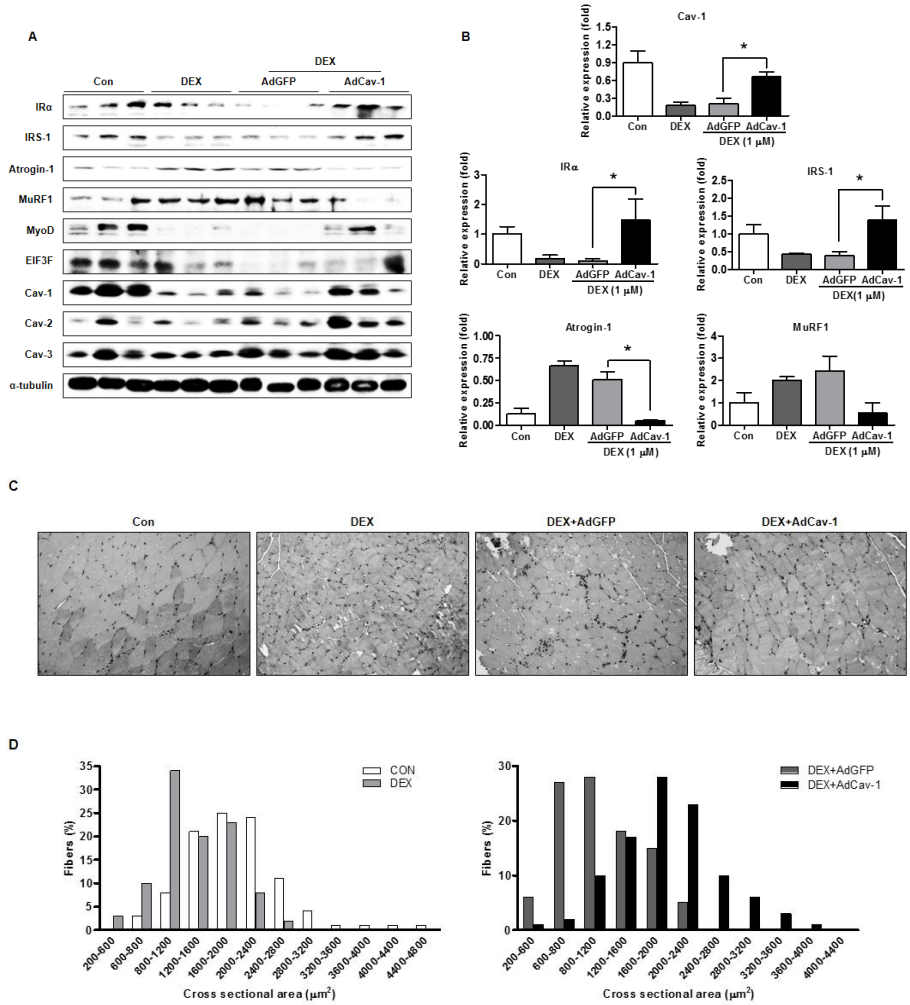

Figure 12. **Caveolin-1 overexpression restores dexamethasone-induced muscle atrophy in mice.** (A) Western blot analysis for caveolin-1 overexpressed gastrocnemius muscle. C57BL/6 mice were treated with every other day i.p. injection of 5 mg kg^{-1} dexamethasone (DEX) or saline (CON) for 12 days, and then treated with daily injection of AdCav1 (DEX-AdCav1) or AdGFP virus (DEX-AdGFP) to gastrocnemius muscle in eight places for 3 days (n = 5 for each group). At sixteenth day, Western blot analyses were performed with gastrocnemius muscle using indicated antibodies. (B) Relative band intensities of Western blot from five mice were estimated by densitometric quantification. Data represent mean ± SD. *P < 0.01 (C) Representative photographs of AdCav1 or AdGFP-injected gastrocnemius muscle from dexamethasone-treated mice. Sections were stained with H&E. (D) The distribution of muscle fiber with different cross-sectional area. Two hundred fibers

per gastrocnemius muscle were randomly chosen and cross-sectional area was measured with a microscope.

-500 tgttccctcaggttcccagccatctcgcttctatatctttctctgtgaaacaaggagacagatc**agttcta**

-420 cgtgggcgaattgggaggggaggcagctt**aggaca**gggcagaattctttctg**cagag**ccggatgcccata

-350 ctgggcatctctgcagactcttgggctccctccacccctgctgagatgatgcactgggaaaacacgcgct

-280 ctcccctggatgcct**ctctg**taggtttatagctgggaaaacgttgcctcgagtctaaaatatctgcccaa

-210 actgcctag**ctctg**atgaaggctttctcacaggctctcagctccccgccggcactccccgcc**ctctg**ctg

-140 ccagaaccttggggatgtgcctagacccggcgcagagcac

— *Putative GRE*

Figure 13. **Sequence of the proximal region of mouse caveolin-1 promoter.** Six putative glucocorticoid-response elements are indicated in the region from -500 to -100 of mouse caveolin-1 promoter.

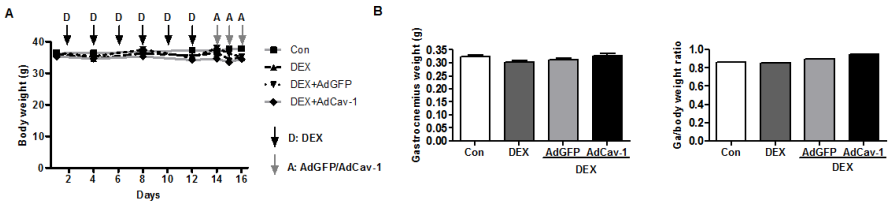

Figure 14. Effects of treatment with dexamethasone and adenovirus on body and gastrocnemius mass in mice. Mice were treated with every other day injection of saline (CON) or dexamethasone (5 mg/kg, DEX) for 12 days, and then treated with daily injection of AdCav1 (DEX-AdCav1) or AdGFP virus (DEX-AdGFP) to gastrocnemius muscle in eight places for 3 days. (A) Total body weight. (B) Gastrocnemius mass. (C) Ratio of gastrocnemius to total body weight. n = 5 for each group.

4. Discussion

Glucocorticoid plays a major role in the development of muscle atrophy observed in many pathological conditions, such as cancer, burn, sepsis and starvation (85). A number of signaling pathways activated by different stimuli is involved in the maintenance of skeletal muscle mass through coordinated regulation of protein synthesis and degradation, including insulin/IGF, myostatin and NFκB pathways (61). Glucocorticoid modulates these pathways via upregulation of several genes, promoting protein degradation and suppressing protein synthesis that result in a decrease in the size of myofibril. Specifically, glucocorticoid inhibits insulin/IGF - PI3K - Akt pathway via upregulation of p85 expression. Inhibition of Akt activity leads to suppression of protein synthesis via mTOR and activation of protein degradation via FOXO transcriptional factor (86). Moreover, glucocorticoid upregulates the expression of REDD1 and KLF15, both of which act as repressors of mTORC1 as well as enhancers for MAFbx/Atrogin-1 and MuRF-1 (65, 66).

In the present study, we showed a new pathway in which glucocorticoid inhibits insulin signaling pathway by down-regulation of Cav1 gene expression. DEX treatment suppresses Cav1 expression in muscle cells, causing a decrease of IRα and IRS-1 and an increase of MAFbx/Atrogin-1 and MuRF-1 protein. Conversely, Cav1 overexpression in mice muscle prevents DEX-induced muscle loss. Our results imply that glucocorticoid effectively inhibits anabolic effect of insulin through negative regulation of upstream components of the signaling pathway. Moreover, results from Cav1 siRNA and overexpression suggest that the inhibition of insulin signaling pathway by glucocorticoid is an important point of control in the maintenance of muscle homeostasis especially under catabolically stressed conditions.

The transcriptional regulation of specific genes by glucocorticoid is dependent on specific GREs. It is well established that GREs have both positive and negative functions (85, 87). Positive GREs activate the transcriptional control of related genes, while negative GREs (nGREs) inhibit them. Our results have identified nGRE for Cav1 gene located at -387 upstream of

promoter region, and showed that this nGRE is responsible for DEX-induced suppression of Cav1 gene by site-directed mutagenesis. Gene expression analyses using microarray showed that a number of genes are downregulated by glucocorticoid (88). However, nGREs are identified in promoter region of only a limited number of genes because nGREs do not have a highly conserved sequence. Moreover, nGREs exhibit inhibitory effect on transcription of target gene in a cell-type specific manner (89). Thus, further studies are required to elucidate the molecular mechanism for tissue-specific suppressive activity of nGREs.

Cav3 is muscle-specific isoform and plays a role in muscle development and physiology by forming a complex with dystrophin and glycoprotein, conferring stability of sarcolemma. Thus, Cav3 deficiency due to mutations in the gene causes the degeneration of myofibril that leads to skeletal muscle diseases (69). Moreover, functional analyses of Cav3-null mice showed that Cav3 is an enhancer of insulin signaling (90). In addition, Cav3 inhibits myostatin signaling by interaction with ALK5, resulting in increased size of myofibers (91). These previous findings suggest that Cav3 could be a plausible target for glucocorticoid. However, contrary to expectation, our results showed that Cav3 protein in mice skeletal muscle was increased rather than decreased in response to DEX-treatment. Interestingly, overexpression of Cav3 also induces muscle fiber degeneration by downregulation of dystrophin (92). Thus, these results together with our data suggest that both increased Cav3 and decreased Cav1expression are likely to contribute to the DEX-mediated muscle atrophy.

Cav1 is abundantly expressed in adipocytes, endothelial cells, type I pneumocytes and smooth muscle cells, and is involved in the pathogenesis of various diseases, including tumorigenesis, diabetes, pulmonary hypertension and hypertrophic cardiomyopathy (93). However, Cav1 has received little attention in muscle biology, despite several reports on the relationship between Cav1 and insulin signaling (74, 94), and skeletal muscle phenotype of Cav1-null mice showing tubular aggregates (95). Our results demonstrated that a reduction in Cav1 levels by DEX-treatment results in muscle atrophy through

suppression of insulin signaling. This finding is consistent with report that Cav1-deficient mice displayed exercise intolerance (96). In this respect, Cav1 may be a key mediator through which glucocorticoid inhibits insulin signaling in muscle tissue.

In summary, our results demonstrated that Cav1 is negatively regulated by DEX through glucocorticoid receptor targeting of nGREs in the promoter region of the gene, and mediates DEX-induced muscle atrophy by regulation of downstream events in the insulin signaling. Thus, these results define a new pathway linking glucocorticoid signaling and insulin pathway in the induction of muscle atrophy, and provide a useful target to prevent the muscle atrophy in steroid therapy.

CHAPTER 3

Role of transglutaminase 2 in skeletal muscle homeostasis

1. Introduction

Skeletal muscle, along with bones and tendons, plays many important biological roles. Skeletal muscle contractions move and stabilize the body. Damage to skeletal muscles, caused by sepsis, denervation, starvation, immobilization, or aging, decreases quality of life. Inactivity owing to chronic disease also reduces independence and quality of life. When the structure or function of skeletal muscle are impeded, the health cost is both personal and national. Thus, muscle damage and disease is closely related to quality of life.

1.1 Skeletal muscle types

Skeletal muscles are comprised of muscle fibers. Muscle fibers consist of myofibrils, the largest subunit of contractile filaments, arranged in parallel. Myofibrils are divided into sarcomeres, the contractile muscle unit, organized end to end. Sarcomeres are made up of two major types of myofilaments, thick and thin (97) (Figure 15). These two types of filaments are composed of the proteins myosin and actin, respectively. The myosin-containing filaments are constituted of myosin heavy chains. Actin is present in all cells and forms the cell structure. Movement is effected by MHC proteins, which can be categorized into four types: slow type I, and fast types IIa, IIb, and IIx. Rodent muscle is composed of all four types, but type IIb is not found in human muscle (98) (Table 1). Slow type I contains many mitochondria for oxidative phosphorylation, as well as high levels of myoglobin. The calcium concentration of slow type muscle oscillates between 100–300 nM, while fast muscle fibers maintain a resting level of 40 nM (99). Calcineurin, a calcium-sensitive serine/threonine phosphatase, activates slow fiberaspecific proteins such as myoglobin in slow muscle fibers, but calcineurin does not activate the fast fiber–specific proteins such as creatine kinase (100). Injection of the calcineurin inhibitor, cyclosporine A (CsA), increases expression of fast fibers from 14% to 31% in the slow muscle of rats (101). A multiprotein complex consisting of muscle transcription factor II repeat domain containing protein 1, TEF-1, and PARP interact with the muscle CAT element of the slow fiber

promoter (102). Various reports have indicated that specific regulatory elements affect the slow muscle fibers. Fast type IIa has a rapid oxidative capacity and is fatigue resistant (103). In rats, these fibers have a higher oxidative capacity than type I fibers, but this is not true in humans (104).

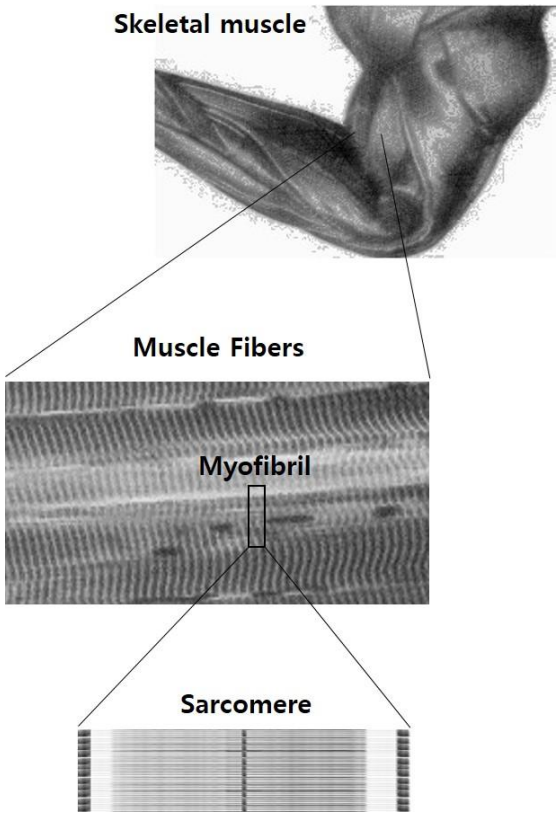

Figure 15. Structure of skeletal muscle is composed of many elongated, parallel fibers, with the myofibrils. The myofibrils showed that repeating banding pattern due to the myosin thick and actin thin filament. These filaments are a single repeat of the banding pattern, referred to a sarcomere. The figure is modified from (97).

muscle type paradigm	References

Two muscle types (fast white muscle and slow red muscle)	**Enzyme histochemistry showes glycolytic and oxidative enzymes in muscle fibers (Dubowitz & Pearse 1960) Cross-reinnervation of fast and slow cat muscles occurs partial conversion of their contractile properties (Buller et al. 1960b). Myosin ATPase activity is higher in fast than in slow muscles and relates with muscle speed of shortening (Barany 1967)**
Three muscle types (Slow 1, Fast 2A, Fast 2B)	**EDL rat muscle have similar fast twith functions (Close 1967), but this muscle contains SDH fibers (Schiaffino et al. 1970) Rat TA muscle contains fast twitch fibers composed of SDH poor and rich fibers (Edstrom & Kugelberg 1968) Mitochondria rich and poor fibers in rat muscles have a more richly developed SR, consistent with a fast twitch (Schiaffino et al. 1970) Idendification of type 1, 2A and 2B fibers by myosin ATPase histochemical staining (Guth & Samaha 1969, Brooke & Kaiser 1970) Fast glycolytic, fast oxidative glycolytic and slow oxidative fibers can be distinguished by enzyme biochemistry (Peter et al. 1972) Enzyme distribution on single human muscle fibers shows differences in SDH avtivity (type 1>2A>2B) and PFK activity (type 2B>2A>1) (Essen et al. 1975)**
Four muscle types (Slow 1, Fast type 2A, Fast type 2X, Fast type 2B)	**Monoclonal and antibodies of MYHs subdivide four MYH isoforms ,including type 2X, and four corresponding fiber types in rat muscle (Schiaffino et al. 1986, 1988, 1989) SDS-PAGE showes the four MYH bands (Bar & Peter 1988, Termin et al. 1989) Identification of type 2X fibers (Larsson et al. 1991b) Identification of a specific 2X MYH gene and distribution of four MYH mRNAs in rat muscles by in sity hybridization (DeNardi et al. 1993) Human muscle fibers seperated as type 2B by ATPase histochemistry contain 2X MYH (Smerdu et al. 1994, Ennion et al. 1995)**
EDL, extensor disitorum longus (a fast-twitch muscle); PFK, phosphofructokinase; MYH, myosin heavy chain; SDH, succinate degydrogenase; SDS-PAGE, sodium	

dodecyl sulphate polyacrylamide gel electrophoresis; SR, sarcoplasmic reticulum; TA, tivialis anterior.

Table 1. Three stages in the developmental notion of skeletal muscle fiber types. The table is derived from (105)

Speed	Slow	Fast	Fast	Fast
MYH	I	IIa	IIx	IIb
Metabolic	oxidative	oxidative	Glycolytic	Glycolytic
Color	Red	Red	White	White
Fibre cross sectional area	Small	Medium	Large	Large
Average % in V.Lateralis muscle				
Human (Andersen et al. 2000)	40	30	30	
Rat (Armstrong & Phelps 1984)	1	36		63
Mouse (Burkholder et al. 1994)	0	30		70
Human do not typically express MHC IIb in skeletal muscle (Smerdu et al. 1994), and both rodent did not show the fast fiber types into IIx and IIb. Thus, IIx fiber are a combination of IIx and IIb.				

Table 2. Common types of skeletal muscle fibers and fiber types percentages in the same muscle across different species. The table is modified from (100).

Mitochondria are highly expressed in type IIa fibers compared with type IIb fibers (100). When AMPK is activated by the ATP/AMP ratio, nuclear respiratory factor-1 (NRF-1) increases the binding activity of the δ-aminolevulinate (ALA) synthase promoter (106). In addition, the ATP/AMP ratio triggers increases in ALA synthase mRNA, cytochrome c protein, and mitochondrial density. AMPK may play an important role in muscle adaptations through the regulation of mitochondrial biogenesis and expression of NRF-1

(106). When mitochondrial function increases, peroxisome proliferator activated receptor coactivator 1 (PGC-1) also increases (107). In this regulatory pathway, PGC-1 increases mitochondrial DAN replication, mitochondrial density, and cytochrome c and cytochrome oxidase (COX) IV protein concentration (107). These serial phenomena show that PGC-1 is the main regulator of muscle type (108). Fast glycolytic fibers (IIx and IIb) have a low mitochondrial density, high glycolytic enzyme activity, high myosin ATPase activity, increased expression of contractile proteins, and low fatigue resistance (100). Fast intrinsic regulatory element (FIRE) is also expressed in fast fibers. The FIRE region contains an E-box, A/T rich site, CACC site, and a CAGG motif (109). The MHC IIb promoter contains A/T rich regions to maintain muscle fiber type specificity.

1.2 Skeletal muscle metabolism

Skeletal muscle contractions mainly consumed energy for ion pumping (110). ATP provides a rapidly available energy source during contraction. The ATP concentration is usually 5–6 mM, but when muscle is activated, the ATP store runs out within 2 s (111). The major anaerobic pathways to generate ATP are degradation of glycogen and phosphocreatine (PCr) (Figure 16).

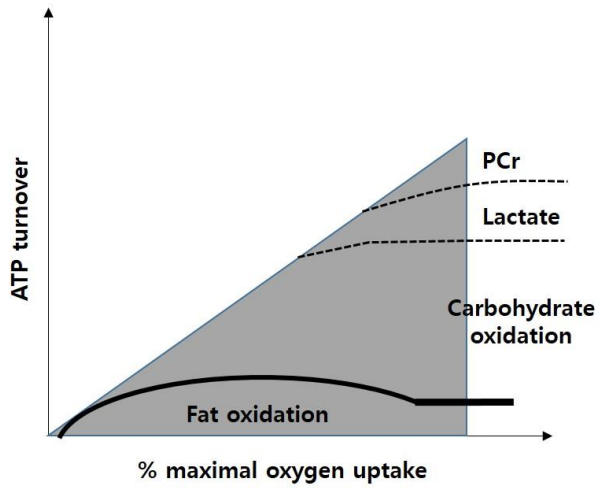

Figure 16. Schematic representation of the relationship between different energy substrates and pathway as a function of exercise intensity. The ATP ratio was estimated in human muscles during cycling. Phosphocreatine (PCr) and lactate

become significant contributors to ATP production only at high exercise intensities. The contribution of protein metabolism is considered to equal zero. The figure is modified from (112)

The PCr degradation reaction, PCr+ADP ↔Cr+ATP, proceeds from left to right during high ATP consumption, resulting in a reduction in PCr and increases in the concentrations of creatine (Cr) and inorganic phosphate ions (Pi), whereas the ATP remains relatively unchanged (112). However, after high ATP consumption, the reaction generally proceeds to the left. Entire muscles do not show a reduction of ATP below 60% but no in maximal cycling exercise (113). Glycogen degradation is regulated by glycogen phosphorylase, which has two forms, phosphorylated and non-phosphorylated. Lactate formation occurs depending on the presence of oxygen. Therefore, lactate accumulates during high-intensity exercise, when ATP consumption is high (114). Oxidative phosphorylation of carbohydrates and lipids constitutes the remaining portion of ATP generation.

The glucose uptake mechanism is not fully understood, but it occurs via an insulin-independent pathway (115). During exercise, AMPK is activated by increasing levels of AMP. Recent studies have shown that muscle contraction during exercise induces production of reactive oxygen species (ROS). ROS production activates AMPK during exercise (116). Free fatty acids form triglycerides that are converted to ATP during high-intensity aerobic exercise (111).

1.3 Hypertrophy

Hypertrophy is an increase in skeletal muscle size, including the cross sectional area (CSA) of muscle fibers. Recent research has expanded the meaning of hypertrophy to include increased contraction, satellite cell proliferation, and new fiber formation (117). The change is based on the balance between protein synthesis and protein degradation. Consequently, a positive or negative balance between synthesis and degradation in the skeletal muscle induces hypertrophy or atrophy, respectively (118). Skeletal muscle can adapt

to various conditions (119). Hard work or resistance exercise results in an increase in muscle size and strength. Understanding the factors regulating muscle mass is important to understand the mechanisms of skeletal muscle maintenance.

1.3.1. Exercise

Exercise, one of the factors that contributes to hypertrophy, is subdivided into resistance exercise and aerobic exercise (Figure 17).

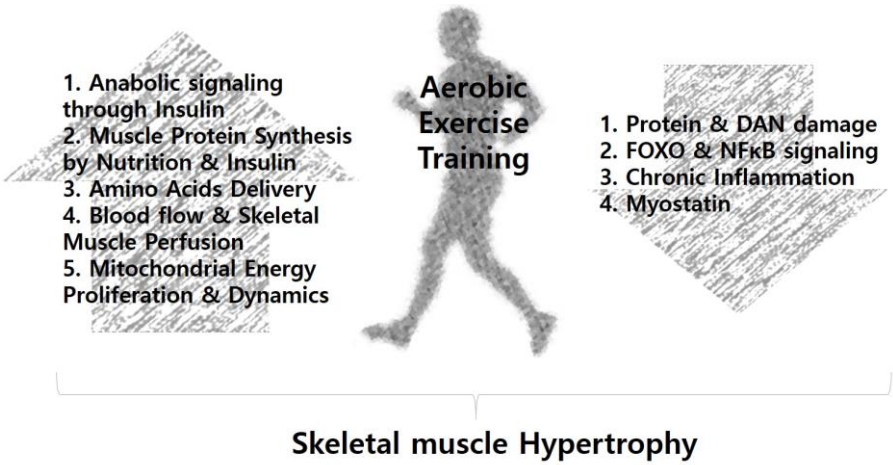

Figure 17. Aerobic exercise training has an effect on many mechanisms that may collectively promote skeletal muscle hypertrophy. The figure is derived from (120).

Both types of exercise physiologically affect muscle mass and capacity. At a molecular level, contraction activates various protein kinases and phosphatases (121). Many protein kinases, such as AMPK, Akt, and the mitogen-activated protein kinases (MAPKs) ERK1/2 and p38, are involved in the regulation of transcription factors (122). These signaling cascades induce chronic nuclear and mitochondrial gene expression, and result in improved endurance, hypertrophy, and force development (123). Contractile activity enhances the p38 MAPK pathway through the phosphorylation of ATF2 (124). In addition, the low-intensity activity of endurance exercise also induces the AMPK-PGC1 system (125). Resistance exercise, in concert with nutrients, growth factors, and mechanical loading, activates the mammalian target of rapamycin (mTOR) to

enhance protein synthesis and cell proliferation. mTORC1, one of the mTOR complexes, is upregulated by amino acid concentrations, resistance exercise, and stress. Mechanical loading (resistance exercise) activates signaling that releases the inhibition of the small G-protein Rheb (a Ras homolog that is enriched in the brain). Rheb then induces activation of mTORC1. After activation of mTORC1, the TSC2 complex (a negative regulator of RHeb) phosphorylates and dissociates from Rheb (126). Thus, like insulin/IGF-1, the activation of mTORC1 phosphorylates TSC2. However, in contrast to insulin/IGF-1, phosphorylation of TSC2 does not activate Akt (118) (Figure 18).

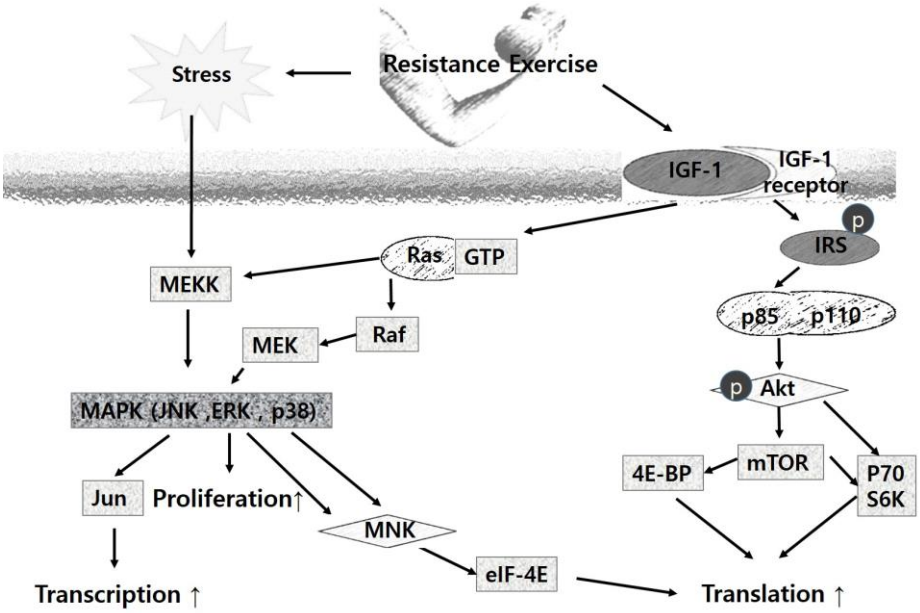

Figure 18. Resistance exercise signaling. IGF-1 receptor is a tyrosine kinase. Activation of IGF-1 receptor by IGF-1 leads its autophosphorylation and initiates a series of events dependent on protein phosphorylation and protein-protein interactions to transmit the IGF-1 signal from the receptor on the plasma membrane to intracellular compartments. Two parallel pathways are involved: one activating PI3K/mTOR and the other activating R/MAP kinase. Several key factors controlling protein transcription/translation are affected by this cascade. mRNA, messenger RNA. The figure is derived from (127).

1.3.2. Hormones

The most well-known regulators of skeletal muscle are hormones such as testosterone, growth hormones, and IGF-1. Hormones each have an individual receptor. When hormones bind to their receptors, they activate a particular pathway. For example, when insulin/IGF-1 binds to its receptor, the receptor activates the insulin receptor substrates 1/2 (IRS 1/2), and IRS1/2 regulates phosphoinositide 3 kinase (PI3K). PI3K changes phosphoinositol (4,5)-bisphosphate into phosphoinositol (3,4,5)-triphosphate. This regulation triggers activation of Akt and its kinase, 3-phosphoinositide dependent protein kinase-1 (PDK1) (128). After activation of Akt, mTOR (mTORC1 and mTORC2) is phosphorylated.

TORC1 is activated in the presence of regulatory-associated protein of mTOR (RAPTOR), whereas mTORC2 binds rapamycin-insensitive companion of mTOR (RICTOR) (118). mTORC2, little effects of rapamycin, phosphorylates Akt at serine 473. mTORC1, which inhibits the effects of rapamycin, activates signaling through the activation of p70S6K and inhibition of 4E-BP1. 4E-BP1 is strictly regulated by mTORC1 (129). During department from 4E-BP1, eIF4E forms a eIF4F complex with eIF4G and eIF4A for translation. This activity is required for formation of the free form of eIF4E and for eIF4G phosphorylation (130). eIF4G is associated with mitogen-activated protein kinase interacting kinases (MNKs) (131). MNK1 and MNK2, which belong to the MNK family, increases phosphorylation in the mTOR dependent manner of IGF1 expression (132). MNK2 negatively regulates the IGF-1/Akt pathway through binding of RAPTOR (133). Unlike dependent of mTOR activation, Akt inactivates glycogen synthase kinase 3 β (GSK3β), which activates the translation initiator eIF2B. GSK3β inhibits skeletal muscle through the transcription factor NFAT (134). When GSK3β is inhibited by Akt, the NFATc1 and C3 proteins move to the nucleus, where they activate myoblast differentiation and a switch to the oxidative fiber type (135).

However, although hormones can affect muscle mass, they have little effect without exercise. Unlike IGF-1–mediated mTOR signaling, guanine nucleotide binding protein (G protein) coupled receptors (GPCRs) regulate skeletal muscle

hypertrophy (136). Four types of G protein receptors (CRFR2, β2-adrenergic receptor (β2AR), LPA receptor, and Fzd7) induce skeletal muscle hypertrophy. G proteins are composed of a GTP-binding alpha subunit (Gα) and a heterodimer of beta and gamma subunits (Gβγ). When Gα binds GTP, phospholipase C and protein kinase C (PKC) are activated. Some reports show that GPCR β2 promotes skeletal muscle atrophy in the presence of mTOR activation by Akt (137, 138). Various studies indicate that hormones require exercise to promote skeletal muscle hypertrophy.

1.3.3. Nutrition

The most effective method to promote muscle growth is eating food. Essential proteins and amino acids increase muscle protein and size. For example, branched-chain amino acids, in particular those that are leucine-rich, activate translation through mTORC1 of various factors including p70 S6 kinase 1 (S6K1) and 4E binding protein-1 (4E-BP1) (139, 140). Similar to hormones, resistance exercise induces muscle hypertrophy with adequate nutrition. However, not all types of food and exercise induce muscle hypertrophy. For skeletal muscle hypertrophy, good dietary habits and high-quality food are required, along with the proper intensity and duration of exercise. Proper nutrition provides the energy source and the components required for protein synthesis.

1.4. Muscle atrophy

Skeletal muscle atrophy, a reduction in mass and/or strength, occurs in various conditions including disuse, denervation, cachexia, sepsis, renal failure, burns, and aging. Striated muscle is directly and indirectly affected by disease mechanisms such as systemic toxicity and inflammation and by the side effects of drugs such as glucocorticoids, statins, radiation, etc. (141-143). Muscle anabolism is activated by growth hormones, insulin, IGF-1, testosterone, exercise, and nutrition. However, muscle catabolism is enhanced by endocrine inflammatory and oxidative stress. Most types of muscle atrophy share a main pathway, and there are three muscle proteolytic mechanisms: (1) the calpain

mechanism (2) the ubiquitin proteasome mechanism and (3) the lysosomal proteasome mechanism (144-146). The caspase mechanism is less related to muscle atrophy, and the closely related muscle apoptosis.

1.4.1. Calpain mechanism

The calpain family comprises nonlysosomal calcium-activated cysteine proteases (147). Three members of the calpain family are expressed in muscle: calpain 1, 2 (μ-calpain), and 3 (highly expressed in skeletal muscle, also known as m-calpain). The μ- and m-calpains are heterodimers that consisted of two subunits of 80 and 30 kDa (148, 149). Because proteolytic activity destroys the cell, calpains are highly regulated (Figure 19).

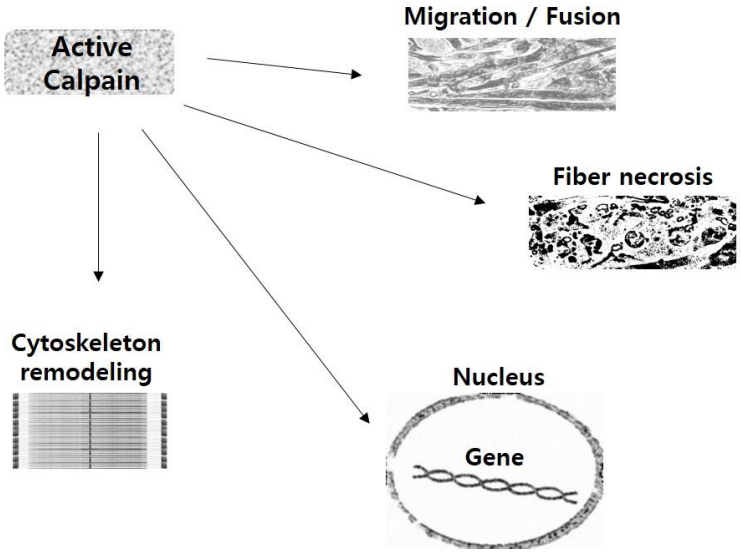

Figure 19. Ubiquitous calpains in atrophy. Upon receiving an activation signal, calpains could play their role in muscle wasting in numerous ways. Activated calpains can degrade sarcomeric proteins, control the expression of several genes by proteolysis of signaling proteins and transcription factors and also may participate in fiber necrosis. In muscle progenitor cells, calpains could control the cell cycle, migration and fusion. The figure is modified from (150).

Calpain is expressed in the cytosol in an inactive form. When the calcium concentration increases, calpain is translocated to the membrane where it is activated by calcium and phospholipids (151). Calcium induces conformational

changes that permit access to the active site (147). When calpain activation degrades the sarcomere, desmin, actinin, titin, and nebulin (152, 153). Calpains may regulate the ubiquitin proteasome system. Increased calpain activity reduces levels of phospho-Akt (S473). Total Akt is not influenced by calcium treatment (147). In addition, calpains regulate transcription factors (STAT, NF-κB, and AP-1) and other regulatory proteins.

1.4.2 Ubiquitin proteasome mechanism (UPM)

The UPM is an ATP-dependent proteolytic system that degrades proteins by conjugation or ubiquitination (154, 155). The conjugation process is regulated by three enzymes: E1 (ubiquitin-activating enzyme), E2 (ubiquitin-conjugating enzyme), and E3 (ubiquitin ligase enzyme). Ubiquitin is transferred from E1 to E2 through the formation of a thioester bond. Subsequently, ubiquitin is transferred from E2 to a lysine residue of the target protein. This step is regulated by the action of E3 (Figure 20). E3s selectively degrade specifically targeted proteins. The ubiquitin complex is recognized by the 26s proteasome, an ATP-dependent proteolytic complex (156).

The muscle-specific E3s, MuRF1 and MAFbx, show increased mRNA and protein levels in fasting, diabetes, cancer, denervation, and immobilization (157, 158). According to some reports, MAFbx degrades the regulatory proteins involved in muscle protein synthesis and regeneration (MyoD1, myogenin, and eukaryotic translation initiation factor 3-subunit (eIF3-f)) (159, 160), while MuRF1 degrades contractile and structural muscle proteins (titin, tropnin1, myosin heavy and light chains, myosin-binding protein C, and proteins related to glycolysis and glycogen metabolism) (161-163) (Figure 21).

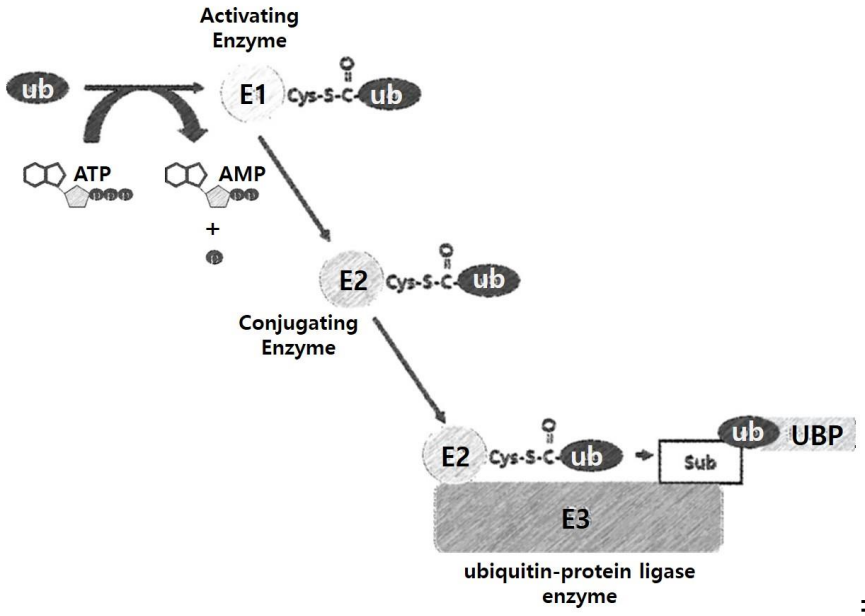

Figure 20. Ubiquitination is a multistep process. Firstly, the E1 ubiquitin activating enzyme binds ubiquitin in an ATP hydrolysis dependent step. Then ubiquitin is transferred from the E1 to the E2 ubiquitin conjugating enzyme. Finally, the E3 ubiquitin-protein ligase enzyme is involved in the formation of a peptide bond between a glycine at the C-terminal of ubiquitin with a lysine of the target protein. Ub detachment is mediated by deubiquitinating enzymes (DUBs). Ubiquitination has diverse outcomes. Polyubiquitination (not shown) leads to protein degradation. For a review discussing diverse forms of ubiquitin modifications. The figure is modified from (164).

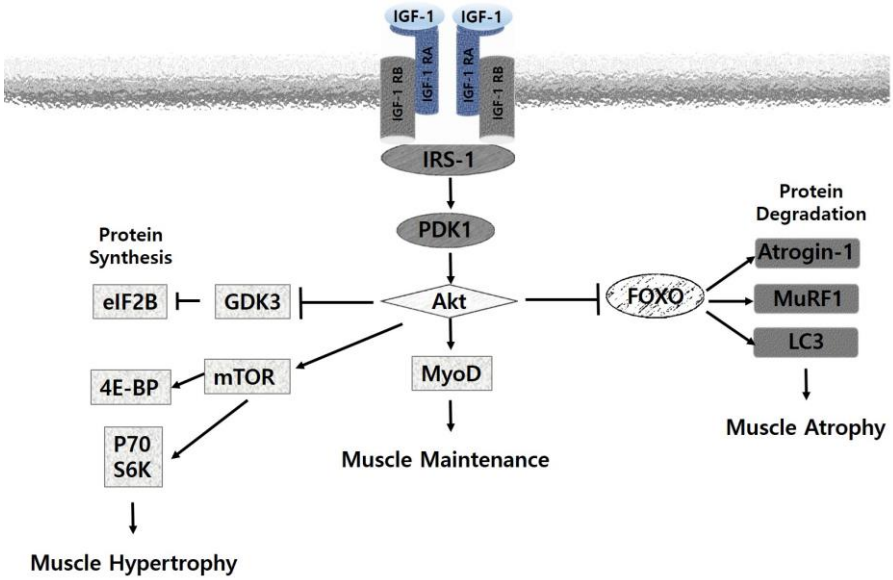

Figure 21. The IGF-1-Akt axis regulates both protein synthesis and protein degradation. Binding of IGF1 to its receptor promotes to phosphorylation of IRS. Phosphorylated IRS recruits and activates PI3K, which in turn recruits PDK1. PDK1 activates Akt by phosphorylation at serine 308. The activated Akt indirectly phosphorylates and activates mTOR kinase. Activated mTOR has two downstream targets which are involved in protein synthesis. It can either phosphorylate the eukaryotic translation initiation factor 4Ebinding protein 1 or it can phosphorylate and activate the S6K1 (p70S6KK kinase) leading in translation initiation. It also controls muscle growth by inactivating the GSK3b which inhibits protein synthesis via the eIF2B, and repressing FOXO signaling. FOXO transcription factors regulate the expression of genes encoding MuRF1 and Arogin-1/MAFbx ligases that lead to muscle atrophy. The figure is derived from (164).

MuRF1 and MAFbx are activated by oxidative stress, inflammatory cytokines (IL-1, TNF-α) and glucocorticoids. These conditions are regulated by p38 mitogen activated protein kinase (MAPK) (124), and nuclear factor kappa B (NF-κB) (165). MAPK is divided into three types: MAPK kinase kinases (MKKKs), MAPK kinases (MKKs), and MAPKs. Oxidative stress and cytokines activate MAPKs (extracellular signal regulated kinases (ERKs) 1/2,

ERK5, c-Jun NH2 terminal kinases (JNKs), and p38s. The p38 MAPK promotes muscle atrophy (165). Interestingly, inhibition of p38 MAPK inhibits overexpression of MAFbx (ref). The mammalian NF-κB family is made up of 5 members, RelA (p65), RelB, c-Rel, NF-κB1 (p50), and NF-κB (p52). In the canonical pathway, NF-κB (p50, and p65) is present in the cytosol in an inactive form with the inhibitor of NF-κBα (IκBα). In muscle atrophy conditions, NF-κBα is activated by IκB kinase (IKK). When IκB proteins are degraded by the 26s proteasome, NF-κB is translocated into the nucleus, where it binds specific DNA sequences in various target genes (166). NF-κB is also activated by a non-canonical pathway, in which NF-κB inducing kinase (NIK) enhances IKKα.

The function of NF-κB in muscle atrophy is to regulate the expression of MURF1 (167). The NF-κB canonical pathway for skeletal muscle atrophy, involving MuRF1 and MAFbx, is well studied, whereas the non-canonical NF-κB pathway remains unclear clear (168).

1.4.3 Lysosomal proteasome mechanism

Lysosomes are membrane-bounded vesicles containing acid hydrolases. Lysosomal hydrolases contain proteases, glucosidases, lipases, nucleases, and phosphatases (169). Lysosomes can degrade cytosol-soluble components, as well as cellular organelles (mitochondria, peroxisomes, and nuclei) (170). Cathepsins L, B, D, and H are the major lysosomal proteases and are ubiquitously expressed in most tissues, but at low levels in skeletal muscles (171, 172). Various conditions, such as fasting, diabetes, cancer, trauma, sepsis, or disuse, increase atrophy via cathepsin L mRNA expression (173). Compared to other cathepsins, cathepsin L increases protein levels of mature and pro-enzyme in catabolic states (174, 175). Glucocorticoid-induced muscle atrophy and disuse atrophy are also associated with cathepsins B and D (175). But, increased expression of the genes encoding cathepsins B and D is not systemically observed in all models of atrophy. Lysosome-dependent degradation of components in the cytosol (autophagy) is related to the vacuolar system and hydrolysis.

1.5. Transglutaminase 2

Transglutaminase 2 (TG2), a member of the transglutaminase family, catalyzes transamidation in the presence of calcium (176, 177). TG2 is responsible for the translational modification of proteins by formation of covalent bonds between free amine groups and γ-carboxyl groups of peptide-bound glutamines (178). TG2 is ubiquitously expressed in all cell types and tissues, and is also referred to as tissue transglutaminase 2 (tTG2). TG2 is predominantly present as a cytosolic protein but is also present in the nucleus and on the plasma membrane. TG2 expression is increased by various signals, such as retinoic acid, vitamin D, TGF-β1, IL-6, tumor necrosis factor (TNF), NF-κB, epidermal growth factor (EGF), phorbol ester, and oxidative stress (179-183).

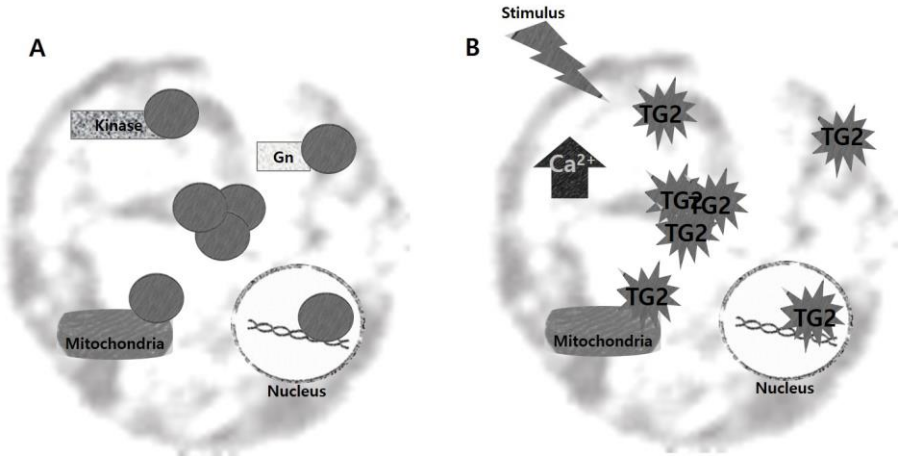

Figure 22. Depending on its subcellular localization, TG2 shows various biochemical activities, such as a transglutaminase, G protein, kinase, PDI. (A) At low calcium concentrations under normal physiological conditions, intracellular TG2 does not show TGase activity, but other activities including Gh, kinase, and PDI. These TG2 enzymatic activities are found in mitochondria, the nucleus, and on the plasma membrane. Extracellular TG2 functions in cell adhesion as an adaptor protein and in ECM remodeling via TGase activity. (B) In response to apoptotic stimuli, elevated calcium concentrations potentiate the TGase activity and suppress all other activities. TGase catalyzes massive intracellular protein crosslinks, generating protective shells that reduce the leakage of intracellular contents of apoptotic cells. During the process, the activated TGase is translocated

to the nucleus, which might mediate chromatin condensation. The figure is derived from (178).

Additionally, TG2 which has transamidation activity, functions similar to GTPase, ATPase, protein kinases, and protein disulfide isomerase (PDI) activity (184) (Figure 22). TG2 also affects phospholipase Cδ, β-integrins, fibronectin, osteonectin, RhoA, multilineage kinases, retinoblastoma protein, PTEN, and IκB (185).

TG2 activity is regulated by various activators. Calcium, guanine nucleotides, and redox potential are the most well-known TG2 regulators (186). TG2 is rendered catalytically inactive by GTP/GDP binding or calcium-induced oxidation, while calcium binding induces TG2 activity. Some thiol reductases also control TG2 activity.

Activated TG2 is associated with a variety of cellular processes, such as differentiation, cell death, inflammation, cell migration, and wound healing. TG2 performs various functions in cells, and is involved in diseases such as celiac disease, neurodegenerative disorders, diabetes, liver cirrhosis and fibrosis, renal scarring, and specific cancers (185). Excessive enzymatic activity of TG2 is considered to be associated with the pathophysiology of several diseases. Therefore, inhibition of TG2 activity is the therapeutic target of these diseases. TG2-knockout mice have no phenotype but show a poor response to stress. TG2 does not show clear activity under normal conditions, either in cell culture or *in vivo*. TG2 protein is an enzyme that only shows activity under stressful conditions. Therefore, an understanding of the biological functions of TG2 may be useful for improving treatment of various diseases.

TG2 has not been studied in skeletal muscle diseases. According to some reports, TG inhibitors block myoblast fusion *in vitro* (187) and TG causes myosin chain crosslinking in some muscles (188).

In this study, we observed severe muscle atrophy in $TG2^{-/-}$ mice. Inhibition of TG2 downregulates the c-Jun, PDK1, and Akt1 axis, resulting in activation of

muscle-specific E3 ligases, MAFbx/atrogin-1, and MuRF-1. Especially, inhibition of TG2 expression and activity regulates c-Jun through translational modification, polyamination, of fbxw7. Our results indicate that TG2 regulates skeletal muscle homeostasis via Fbxw7.

2. Materials and Methods

2-1. Cell culture

C2C12 cells were purchased from American type culture collection. And we cultured and differentiated previously (189).

2-2. Western blot analysis

Cells were lysed as described previously (189). Equal amounts of proteins were transferred to nitrocellulose membrane and probed with an ECL Kit (Pierce, Rockford, IL, USA). The signal intensity was determined using an LAS-3000 image reader (Fujifilm, Tokyo, Japan). We probed with following antibodies: MAFbx, MuRF1 (ECM bioscience, Versailes, KY, USA), FBXW7, Spermine (Abcam, Cambrige, MA, USA), α-tubulin (Sigma-Aldrich), MyoD, c-Jun, Cyclin E1, C-myc, Notch1 (Santa Cruz Biotechnology), Akt, p-Akt (S473, T308), Foxo1a, p-Foxo1a, NF-κB, p- NF-κB, IκB, P110α, p85, PDK1, mTOR, pmTOR, pS6K, p-c-Jun (S63), GSK3β, p-GSK3β, JNK, pJNK (Cell signaling technology)

2-3. Real-time quantitative RT-PCR

Total RNA was isolated from C2C12 myotubes using the E.Z.N.A. Total RNA Kit (Omega Bio-Tek inc., Norcross, GA, USA), and the expression levels of MAFbx/Atrogin1, MuRF1, PDK1, TG2, FBXW7 (α, β, and γ) and 34B4 mRNA were assessed by qPCR using an iCycler RT-PCR instrument (Bio-Rad). The following specific primers were used: MAFbx/Atrogin1, 5-CTCTGTACCATGCCGTTCCT- 3, (forward) and 5-GGCTGCTGAACAGA TTCTCC- 3 (reverse); MuRF1, 5-TGTCTGGAG GTCGTTTCC G-3, (forward) and 5-TGCCGGTCCATGATCACTT-3 (reverse); PDK1, 5-ACCTACCAG CCATGTCAGAGGATG-3, (forward) and 5-AACTGGCTCA GGAGATT GTCGTAG-3 (reverse); FBXW7α, 5-AGTAGTAT TGTGGACCTGCCCGTT-3, (forward) and 5-GACCTCAGAACCATGGTCCAACTT-3 (reverse); FBXW7β, 5-TATTGTCAGAGACTGCCAAGCAGC-3, (forward) and 5-GACCTCAGAACCATGGTCCAACTT (reverse); FBXWγ, 5-CCATGGC

TTGGTTCCTGTTGATCT-3, (forward) and 5-GCCTTGGGCAATGATGC TAATGCT-3 (reverse); 34B4, 5-TCCAGGCTTTGGGCATCA-3. (forward) and 5-CTTTATCAGCTGCACATCAC TCAGA-3 (reverse)

2-4. Cell transfection and luciferase assays

C2C12 myotubes were plated in 12-well. The cells were transfected PDK1 promoter wild type and mutation type (190) with lipofectamine 2000 (Invitrogen, Life Technologies). After differentiation, The Myotubes were differentiated for 4 days and the treated with KCC009 250μM and TG2 siRNA for 24h. After preparation of the myotubes lysates, we performed the luciferase activity with dual-luciferase reporter assay system (Promega). The results are expressed at the mean ±S.D. of at least five independent experiments.

2-5. Immunoprecipitation

Immunoprecipitation was performed using the magnetic beads (Millipore) according to the manufacturer's instructions. Cell lysates incubated with FBXW7, spermine, and IgG antibody for 1hours in 4℃ temperature. During incubation with Antigen and Antibody, gently mix the beads suspension and pipetting 50μl of suspended beads into a 1.5ml e-tube. After cold incubation, Mixture of antigen and antibody placed with magnetic beads for 1 hour at rotating rod. Magnetic beads plus mixture place the tube into the magnetic stand, allow the beads to migrate to the magnet, and then remove the buffer with a pipette. Wash the beads 3 times with PBS. After the wash, remove the tube from the stand and add the 1X sample buffer. Boiling the 1Xsample buffer at 100℃ temperature.

2-6. siRNA Knockdown of TG2 and PDK1

TG2 and PDK1 specific siRNA was purchased from Santa Cruz Biotechnology siRNA (10nM) was transfected into Myotubes for 10min using the G-fectin transfection protocol previously (189).

2-7. Measurement of myotube diameter

After differentiation, myotubes were stained using PAS staining kit (Merck). All experiments performed previously (189).

2-8. Animals

C57BL/6J mice were purchased from the Jackson laboratory. $TG^{-/-}$ mice were generated with C57BL/6J backcrossing. All animal procedures were approved by the Institutional Animal Care and Use Committee of the Seoul National University College of Medicine.

2-9. Treadmill exercise test

Two group mice ($TG^{+/+}$, $TG^{-/-}$) performed the treadmill exercise test (191, 192) The treadmill was equipped with electric shock bars at the rear of the belt to stimulate mouse to run. Mice ran on a treadmill starting at a warm-up speed of 5m/min for 5 minutes. After adaptation for one week, exhausting exercise test began 3m/min belt speed and Belt speed was faster linearly by 3m/min every 3min until 15m/min were reached.

2-10. Measurement of muscle fiber cross-sectional area

Muscle samples were fixed with 4% paraformaldehyde, and made the glass slide samples stained with H&E. Muscle fiber cross sectional area (CSA) were visualized and captured with a microscope camera (Zeiss). At least 200 fibers per one muscle were randomly analyzed using Image J program.

2-11. Statistical analyses

All statistical calculations were performed using GraphPad Prism version 5.0 (GraphPad Software, San Diego, CA, USA).

3. Results

3.1. $TG^{-/-}$ mice show muscle atrophy and decreased the muscle function.

The total body weight of $TG^{-/-}$ mice was not significantly reduced; however, the gastrocnemius muscle (GA) weight of $TG^{-/-}$ mice was lower than that of $TG^{+/+}$ mice (Figure 23A). Consistently, H&E staining and cross-sectional area (CSA) of GA muscle (Figure 23B, C) showed a dramatic reduction of fibers *in vivo*. To confirm physiological function in $TG^{-/-}$ mice, we performed grip strength and exercise tolerance tests (Figure 23D, E). In the grip strength test, the front paws of $TG^{-/-}$ mice did not show any decrease in force, while the rear paws were weaker than in $TG^{+/+}$ mice. As expected, running distance and duration of $TG^{-/-}$ mice were shorter (40% and 50%, respectively) than those of $TG^{+/+}$ mice in the exhaustion test. These data indicated that $TG^{-/-}$ mice showed severe GA muscle atrophy.

3.2. TG2 deficiency suppressed insulin signaling and activated protein degradation

To investigate the function of TG2 in muscle atrophy, we evaluated levels of muscle atrophy and protein synthesis markers in the GA muscle of $TG^{-/-}$ mice. It is well known that atrogin-1 and MuRF1 are the main E3 ligases of muscle atrophy in specific muscle atrophy conditions. Western blot analysis showed that ablation of TG2 increased atrophy markers and decreased MyoD, the substrate of atrophy markers, in GA muscle. In muscle catabolic conditions, Foxo1 and NF-κB, upregulators of catabolism signaling, promote muscle atrophy markers (atrogin-1, and MuRF1). Thus, we next examined protein levels of Foxo and NF-κB in the GA muscle of $TG^{-/-}$ and $TG^{+/+}$ mice. Protein expression of Foxo1 was not altered, while NF-κB activity increased (Figure 24A, B). Muscle atrophy results from an imbalance between protein synthesis and protein degradation. To confirm the reduction of protein synthesis, we measured insulin-related signaling. Expression of PI3K subunits (P110a and P85) increased, but the expression of downstream proteins (pAkt, PDK1, and pS6K) was significantly decreased in GA muscle (Figure 24C, D). Thus, these

results clarified that ablation of TG2 induced muscle atrophy through the imbalance of protein degradation and protein synthesis.

3.3. PDK1 is a regulator of skeletal muscle homeostasis

To study of the function of PDK1 in myotubes, C2C12 myotubes were treated with PDK1-specific siRNA or scrambled siRNA for 24 h (Figure 25A). We observed a 50% reduction of muscle fiber diameter in myotubes treated with PDK1 siRNA in comparison with those treated with scrambled. In the PDK1 siRNA treatment, pAkt (S473, T308) was significantly decreased, but atrogin-1 and MuRF1, muscle atrophy markers, were higher than in the scrambled treatment (Figure 25B). To determine the effect of PDK1 siRNA transfection at the transcriptional level, we performed qPCR (Figure 25C) and found that atrogin-1 and MuRF1 mRNA were increased significantly. To confirm the inhibitory effect of PDK1, we administered various doses of GSK2334470 (0.1, 1, 10 μM) for 24 h (Figure 3D, 3E). We observed a reduction of muscle fiber diameter as the concentration of GSK2334470 increased (Figure 25D). As expected, two proteins phosphorylated by Akt (S473, T308) were decreased, but atrogin-1 and MuRF1 were increased.

3.4. TG2 controls PDK1 levels through c-Jun

To confirm the transcriptional regulation of PDK1 by TG2, we used two promoter mutation constructs (M1Δ2, M3) of c-Jun binding sites in PDK1. Mutation constructs were fused with a luciferase reporter and transfected into myotubes (Figure 26A). Scrambled-treated cells increased the luciferase activity of WT constructs while TG2 siRNA–treated cells showed no significant effect (Figure 26B). To confirm the c-Jun binding sites of the PDK1 promoter in TG2 inhibitor–treated myotubes, we administered the TG2 inhibitor, KCC009, at two different doses (100, 250μM). KCC009 did not show any effect on luciferase activity, while the control showed increased luciferase activity (4-fold) (Figure 26C). We next investigated the effect of KCC009 at various time points (0, 3, 6, 9, 12, 15, 18, 21, 24 h). The level of c-Jun decreased in a time-dependent manner. PDK1, pAkt (S473, T308), and pGSK3β also decreased in

a time-dependent manner (Figure 26D). Finally, to verify the relationship between TG2 and muscle atrophy in myotubes, we administered KCC009 at two different doses (100, 250 μM) (Figure 4E) and TG2 siRNA (Figure 26F). Both KCC009 and TG2 siRNA samples showed a similar effect: protein levels of atrogin-1 and MuRF1 increased, while PDK1 expression dramatically decreased.

3.5. c-Jun is degraded by TG2 suppression in myotubes

To examine the regulation of c-Jun signal transduction, we measured protein and mRNA levels of JNK, a direct regulator of c-Jun, in KCC009-treated cells (Figure 27A). Protein levels of c-Jun were reduced by KCC009, but the JNK protein level did not change, nor did c-Jun mRNA levels change. To confirm the specific inhibition of TG2, we administered TG2 siRNA to myotubes. Similarly, TG2 siRNA showed a reduction of c-Jun protein levels, but c-Jun mRNA did not show any difference (Figure 27B). Therefore, to confirm the proteolytic degradation of c-Jun, we performed MG132 cotreatment with KCC009. MG132 prevented c-Jun degradation by KCC009 (Figure 27C). To determine the specific ubiquitin E3 ligase responsible, we screened target proteins of two ubiquitin E3 ligases (Fbxw7, Mekk1) during KCC009 treatment. Cyclic E1 of the Fbxw7 target protein was degraded by KCC009 (Figure 27D). However, protein and mRNA levels of Fbxw7 remained unchanged following KCC009 treatment (Figure 27E).

3.6. Fbxw7 is a substrate for TG2

To investigate the direct interaction between Fbxw7 and TG2, we performed immunoprecipitation. Spermine antibody indicates the endogenous function of TG2. The integrity between Fbxw7 and endogenous TG2 activity was decreased in myotubes with KCC009 treatment (250 μM) (Figure 28A, B). To further study this phenomenon *in vivo,* we performed immunoprecipitation in wild-type and TG2-KO mice. The interaction between Fbxw7 and Spermine was reduced, suggesting that TG2 is the regulator of Fbxw7.

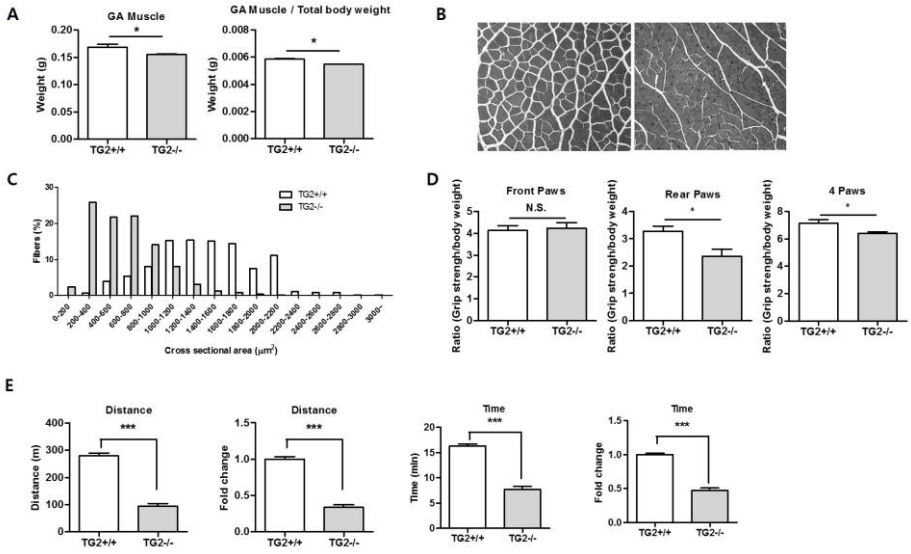

Figure 23. TG$^{-/-}$ mice exhibit decreased skeletal muscle mass

Gastrocnemius muscle (GA) muscle weight was significantly lower in TG$^{-/-}$ mice (n = 8) than in control mice (n = 8). Also, when normalized to total body weight, the GA muscle weight of TG$^{-/-}$ mice was significantly lower than in controls. (B) GA muscles were prepared for H&E staining. Scale bars: 200 μm. (C) The cross-sectional area (CSA) of the GA muscle from TG$^{-/-}$ mice was smaller than that of control mice. (D) The front paw strength of TG$^{-/-}$ mice was not significantly different from that of control mice, although rear paw strength was significantly decreased. When normalized to total body weight, the grip strength of TG$^{-/-}$ mice was significantly reduced.

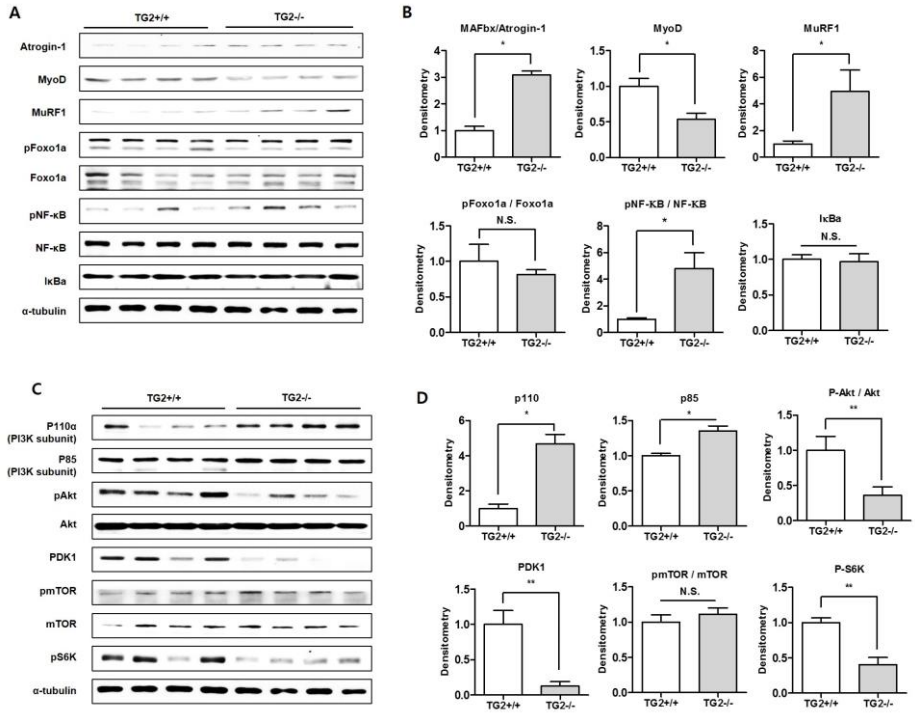

Figure 24. TG2 deficiency suppresses insulin signaling by inhibiting PDK1 expression

(A) Western blot analysis of gastrocnemius muscle using muscle atrophy markers. (B) Relative band intensities from four mice were estimated by densitometry. Data are presented as mean (S.D.) *P < 0.01 (C) Western blot analysis of gastrocnemius muscle using protein synthesis markers. (D) Relative band intensities from four mice were estimated by densitometry. Data are presented as mean (S.D.) *P < 0.01

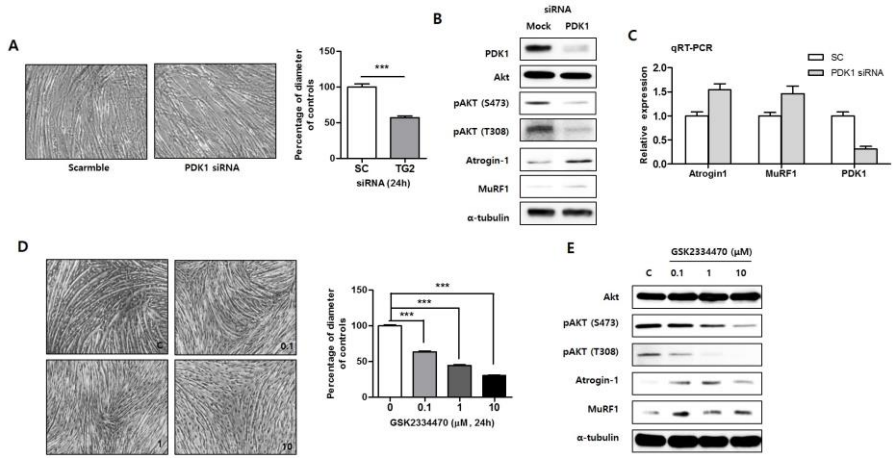

Figure 25. PDK1 is critical for muscle homeostasis.

(A) PAS staining images of myotubes treated with PDK1 siRNA and scrambled siRNA. Scale bars: 100 μM. (B) Western blot analyses of PDK1 siRNA and scrambled siRNA samples using antibodies against PDK1, Akt, pAkt (S473), pAkt (T308), atrogin-1, MuRF1, and α-tubulin. (C) Total RNA from myotubes treated with PDK1 siRNA or scrambled siRNA for 24 h was analyzed by qPCR for atrogin-1, MuRF1, and PDK1. (D) PAS staining images of myotubes treated with GSK2334470 (PDK1 inhibitor, 0.1 μM, 1 μM, and 10 μM) for 24 h. (E) Western blot analysis of myotubes treated with GSK2334470, using antibodies to Akt, pAkt (S473), pAkt (T308), atrogin-1, MuRF1, and α-tubulin.

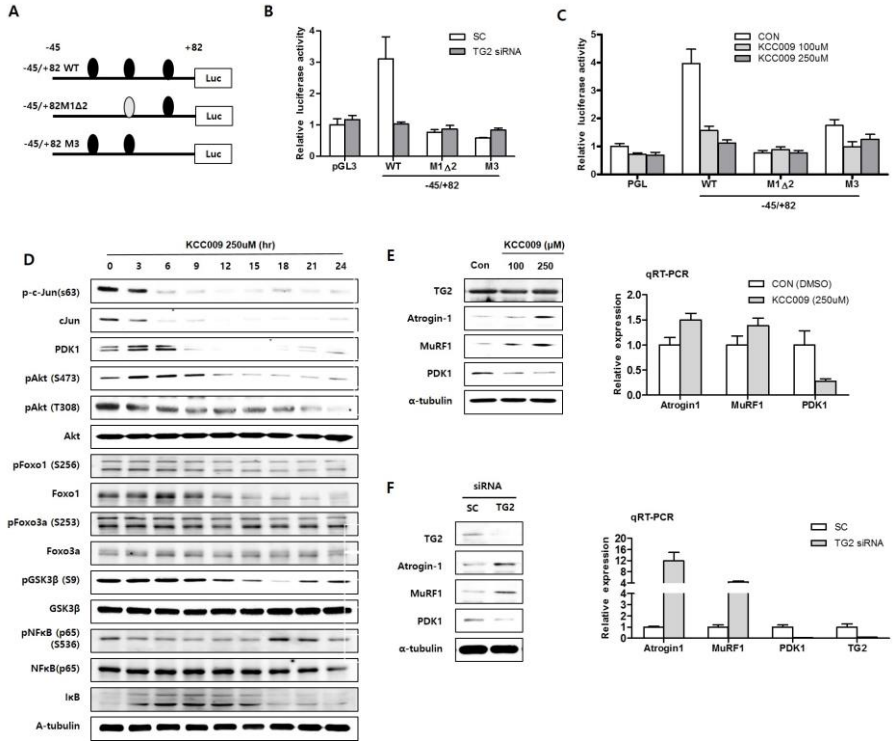

Figure 26. TG2 regulates PDK1 expression through c-Jun

(A) Schematic image of the c-Jun binding sites in the PDK1 promoter. (B) Luciferase reporter activity of mutation constructs of the PDK1 promoter. Myotubes cotransfected with mutation constructs and TG2 siRNA. (C) Reporter assay activity in KCC009 (TG2 inhibitor) treatment samples. (D) Myotubes were treated with KCC009 (250 μM) at various time points. Cell lysates were analyzed by western blotting using antibodies against p- c-Jun (S63), c-Jun, PDK1, pAkt (S473), pAkt (T308), Akt, pFoxo1 (S256), Foxo1, pFoxo3a (S253), Foxo3a, pGSK3beta (S9), GSK3beta, pFN-kB (S536), NF-κB, IκB, and α-tubulin. (E) Myotubes were treated with KCC009 (100 μM, 250 μM). Western blot analyses of myotubes treated with antibodies against TG2, atrogin-1, MuRF1, PDK1, and α-tubulin. Atrogin-1, MuRF1, and PDK1 expression in myotubes as measured by qPCR. (F) Myotubes were transfected with TG2 siRNA or scrambled siRNA. Western blot analyses of myotubes treated with antibodies against TG2, atrogin-1, MuRF1, PDK1, and α-tubulin. Atrogin-1, MuRF1, PDK1, and TG2 expression in myotubes as measured by qPCR.

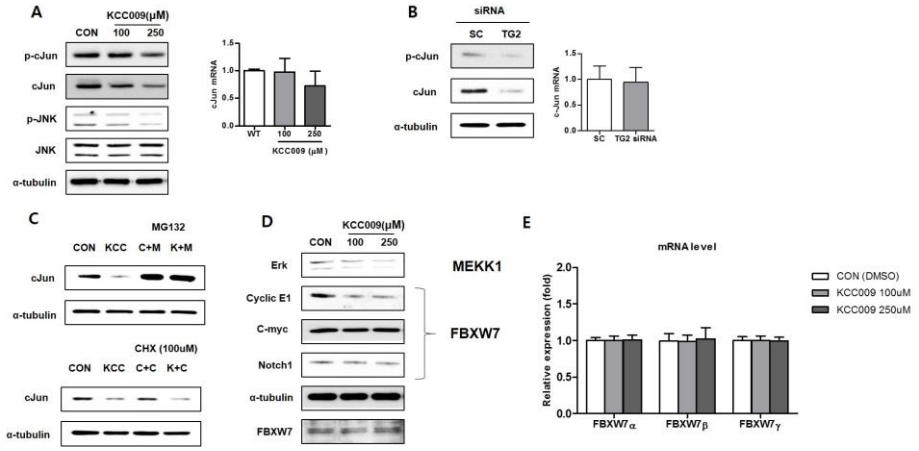

Figure 27. c-Jun is degraded by Fbxw7 in TG2-suppressed C2C12 myotube cells

(A) Myotubes were treated with KCC009 (100 μM, 250 μM). Western blot analyses of myotubes treated using antibodies against c-Jun, p-c-Jun, JNK, p-JNK, and α-tubulin. c-Jun expression in myotubes as measured by qPCR. (B) Myotubes were transfected with TG2 siRNA or scrambled siRNA. Western blot analyses of myotubes treated with antibodies against c-Jun and α-tubulin. c-Jun expression in myotubes as measured by PCR. (C) Myotubes were incubated in the presence of KCC009 or MG132, and the expression of c-Jun and α-tubulin was determined by western blotting. Myotubes were treated with KCC009 or cycloheximide, and the expression of c-Jun and α-tubulin was measured by western blotting. (D) Western blot analyses of myotubes treated using antibodies against Erk, Cyclic E1, c-myc, Notch1, and α-tubulin. (E) qPCR analysis of Fbxw7 isotype (a, b, and r) mRNA in KCC009-treated C2C12 myotubes.

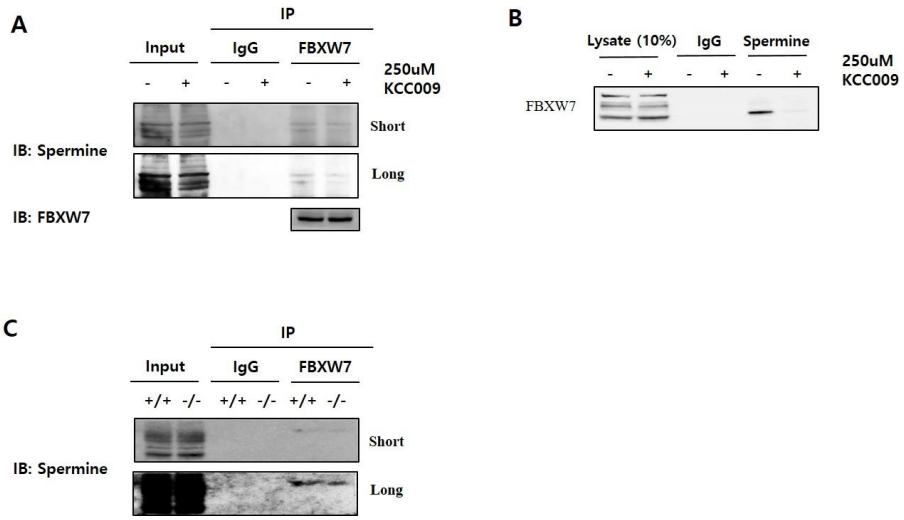

Figure 28. TG2 inhibits Fbxw7 by polyamination

Myotubes were treated with KCC009 (250 μM). Immunoprecipitated (IP) Fbxw7 from cell extracts were determined by western blotting. (B) IP spermine from cell lysates were analyzed by immunoblotting with Fbxw7 antibody. (C) IP Fbxw7 from GA muscle of $TG^{-/-}$ mice was analyzed by immunoblotting with anti-spermine.

4. Discussion

Transglutaminase 2 (TG2) is a cross-linked enzyme in Ca^{2+}-dependent and stressed conditions (178, 183). This enzyme is ubiquitously present in every organ; however, its function in skeletal muscle is not clear. Muscle homeostasis is regulated by the ratio of protein synthesis and degradation. Many studies have shown that the insulin and PI3K pathways are the main pathways for regulation of muscle mass (117, 118, 120, 127). However, regulation of skeletal muscle homeostasis is not fully understood. TG2-KO do not appear to differ from wild-type mice. However, using $TG^{-/-}$ mice, we discovered a role for TG2 in the skeletal muscle mass via the Fbxw7-c-Jun-PDK1-Akt axis. The results of physiological testing indicated that TG2 deficiency caused muscle loss, including reduction of muscle fiber. Moreover, in the grip strength and exercise acute tolerance tests, $TG^{-/-}$ mice were shown to be severely deficient. These *in vivo* physiological data are consistent with the association between TG2 and skeletal muscle.

In muscle atrophy studies, many researchers have confirmed the identity of skeletal muscle atrophy markers and proteolytic pathways (141, 143, 144, 154, 159, 160, 162). We showed that the specific atrophy markers, atrogin-1 and MuRF1, were increased in GA muscle of $TG^{-/-}$ mice. In proteolysis of skeletal muscle, specific atrophy markers are controlled by upregulators, such as Foxo and NF-κB in atrophic conditions. NF-κB increased dramatically, as expected, but Foxo did not show any difference in TG2-KO mice. This result showed that ablation of TG2 induced NF-κB–mediated muscle atrophy, but not Foxo-mediated muscle atrophy.

Next, we find that expression of the PI3K subunits P110, P85 were increased in TG2KO mice. Physiologically, increased proteolysis induced the compensatory PI3K pathway to maintain skeletal muscle homeostasis (193). In contrast with this regulation, protein synthesis was reduced through the PDK1-Akt-S6K axis in GA muscle of TG2KO mice. We observed accelerated muscle atrophy resulting from the increased protein degradation and decreased protein synthesis. It was not fully elucidated that the reduction of PDK1 induced muscle

atrophy. As in TG2-KO mice, we observed similar expression of both muscle atrophy and protein synthesis markers in myotubes following treatment with PDK1 siRNA and PDK1 inhibitors. These results showed that PDK1 is an important protein in muscle atrophy. A previous study showed that c-Jun regulates PDK1 transcription in cancer cells (190); however, this regulation has not been investigated in skeletal muscle. We observed that the TG2 inhibitor and TG2 siRNA decreased *PDK1* luciferase activity via the c-Jun binding site in C2C12 myotubes. In other words, inhibition of TG2 decreased PDK1 transcription via c-Jun in skeletal muscle. Thus, we inferred that c-Jun regulates PDK1 in skeletal muscle; we also confirmed that TG2 regulates PDK1 through c-Jun in skeletal muscle. According to previous reports, various proteins regulate c-Jun signaling (194, 195). Contrary to previous reports, c-Jun changed first, and then the PDK1-Akt axis was reduced via TG2 inhibition in C2C12 myotubes in a time-dependent manner. Further, as in $TG^{-/-}$ mice, muscle atrophy occurs by inhibition of TG2 *in vitro*. These serial data indicated that TG2 directly affects protein synthesis through c-Jun signaling in skeletal muscle.

The transcription and stability of c-Jun are affected by JNK (196-198). However, we did not observe that TG2 affects JNK. Nor did TG2 decrease the transcription level of c-Jun. Treatment with MG132, a proteasome inhibitor, provides strong evidence that c-Jun is degraded by two ubiquitin E3: Fbxw7 and Mekk1. The function of these E3 ligases in skeletal muscle has not been reported. We observed that the substrate (Cyclin E1) of Fbxw7 was decreased by the TG2 inhibitor, although the substrate of Mekk1 did not change. Furthermore, the TG2 inhibitor did not affect protein or mRNA levels of Fbxw7.

Spermine is an antibody that indicates the activity of TG2. If polyamination occurs in proteins via TG2, spermine levels would be altered. Fbxw7 levels were decreased by addition of a TG2 inhibitor in C2C12 myotubes. Furthermore, this phenomenon was concordant with the pattern observed in GA muscle of $TG^{-/-}$ mice. Therefore, our data suggest that Fbxw7 is post-translationally modified by TG2.

Further studies are required to clarify the specific site at which TG2 modifies Fbxw7. In summary, our data showed that TG2 regulates muscle homeostasis

via Fbxw7 in skeletal muscle. Taken together, our findings show a new pathway and provide therapeutic target in skeletal muscle atrophy.

References List

1. Iismaa SE, Mearns BM, Lorand L, Graham RM. Transglutaminases and disease: lessons from genetically engineered mouse models and inherited disorders. Physiological reviews. 2009;89(3):991-1023.
2. Nurminskaya MV, Belkin AM. Cellular functions of tissue transglutaminase. Int Rev Cell Mol Biol. 2012;294:1-97.
3. Shin DM, Jeon JH, Kim CW, Cho SY, Kwon JC, Lee HJ, et al. Cell type-specific activation of intracellular transglutaminase 2 by oxidative stress or ultraviolet irradiation: implications of transglutaminase 2 in age-related cataractogenesis. The Journal of biological chemistry. 2004;279(15):15032-9.
4. Siegel M, Strnad P, Watts RE, Choi K, Jabri B, Omary MB, et al. Extracellular transglutaminase 2 is catalytically inactive, but is transiently activated upon tissue injury. PLoS One. 2008;3(3):e1861.
5. Jang GY, Jeon JH, Cho SY, Shin DM, Kim CW, Jeong EM, et al. Transglutaminase 2 suppresses apoptosis by modulating caspase 3 and NF-kappaB activity in hypoxic tumor cells. Oncogene. 2010;29(3):356-67.
6. Szondy Z, Korponay-Szabo I, Kiraly R, Fesus L. Transglutaminase 2 dysfunctions in the development of autoimmune disorders: celiac disease and TG2-/- mouse. Adv Enzymol Relat Areas Mol Biol. 2011;78:295-345.
7. Klock C, Diraimondo TR, Khosla C. Role of transglutaminase 2 in celiac disease pathogenesis. Semin Immunopathol. 2012;34(4):513-22.
8. Sollid LM, Jabri B. Celiac disease and transglutaminase 2: a model for posttranslational modification of antigens and HLA association in the pathogenesis of autoimmune disorders. Curr Opin Immunol. 2011;23(6):732-8.
9. Oh K, Park HB, Byoun OJ, Shin DM, Jeong EM, Kim YW, et al. Epithelial transglutaminase 2 is needed for T cell interleukin-17 production and subsequent pulmonary inflammation and fibrosis in bleomycin-treated mice. The Journal of experimental medicine. 2011;208(8):1707-19.
10. Oh K, Park HB, Seo MW, Byoun OJ, Lee DS. Transglutaminase 2 exacerbates experimental autoimmune encephalomyelitis through positive regulation of encephalitogenic T cell differentiation and inflammation. Clinical immunology. 2012;145(2):122-32.
11. Luciani A, Villella VR, Vasaturo A, Giardino I, Pettoello-Mantovani M, Guido S, et al. Lysosomal accumulation of gliadin p31-43 peptide induces oxidative stress and tissue transglutaminase-mediated PPARgamma downregulation in intestinal epithelial cells and coeliac mucosa. Gut. 2010;59(3):311-9.
12. Maiuri L, Luciani A, Giardino I, Raia V, Villella VR, D'Apolito M, et al. Tissue transglutaminase activation modulates inflammation in

cystic fibrosis via PPARgamma down-regulation. Journal of immunology. 2008;180(11):7697-705.
13. Falasca L, Farrace MG, Rinaldi A, Tuosto L, Melino G, Piacentini M. Transglutaminase type II is involved in the pathogenesis of endotoxic shock. Journal of immunology. 2008;180(4):2616-24.
14. Danese S, Fiocchi C. Ulcerative colitis. N Engl J Med. 2011;365(18):1713-25.
15. Baumgart DC, Sandborn WJ. Crohn's disease. Lancet. 2012;380(9853):1590-605.
16. Van Limbergen J, Radford-Smith G, Satsangi J. Advances in IBD genetics. Nat Rev Gastroenterol Hepatol. 2014;11(6):372-85.
17. Duerr RH, Taylor KD, Brant SR, Rioux JD, Silverberg MS, Daly MJ, et al. A genome-wide association study identifies IL23R as an inflammatory bowel disease gene. Science. 2006;314(5804):1461-3.
18. Barrett JC, Hansoul S, Nicolae DL, Cho JH, Duerr RH, Rioux JD, et al. Genome-wide association defines more than 30 distinct susceptibility loci for Crohn's disease. Nature genetics. 2008;40(8):955-62.
19. Jostins L, Ripke S, Weersma RK, Duerr RH, McGovern DP, Hui KY, et al. Host-microbe interactions have shaped the genetic architecture of inflammatory bowel disease. Nature. 2012;491(7422):119-24.
20. Farrace MG, Picarelli A, Di Tola M, Sabbatella L, Marchione OP, Ippolito G, et al. Presence of anti-"tissue" transglutaminase antibodies in inflammatory intestinal diseases: an apoptosis-associated event? Cell Death Differ. 2001;8(7):767-70.
21. Ni J, Chen SF, Hollander D. Effects of dextran sulphate sodium on intestinal epithelial cells and intestinal lymphocytes. Gut. 1996;39(2):234-41.
22. Berndt BE, Zhang M, Chen GH, Huffnagle GB, Kao JY. The role of dendritic cells in the development of acute dextran sulfate sodium colitis. Journal of immunology. 2007;179(9):6255-62.
23. Okayasu I, Hatakeyama S, Yamada M, Ohkusa T, Inagaki Y, Nakaya R. A novel method in the induction of reliable experimental acute and chronic ulcerative colitis in mice. Gastroenterology. 1990;98(3):694-702.
24. Goldberg R, Prescott N, Lord GM, MacDonald TT, Powell N. The unusual suspects-innate lymphoid cells as novel therapeutic targets in IBD. Nat Rev Gastroenterol Hepatol. 2015;12(5):271-83.
25. Dafik L, Albertelli M, Stamnaes J, Sollid LM, Khosla C. Activation and inhibition of transglutaminase 2 in mice. PLoS One. 2012;7(2):e30642.
26. Araya RE, Jury J, Bondar C, Verdu EF, Chirdo FG. Intraluminal administration of poly I:C causes an enteropathy that is exacerbated by administration of oral dietary antigen. PLoS One. 2014;9(6):e99236.
27. Yoo H, Ahn ER, Kim SJ, Lee SH, Oh SH, Kim SY. Divergent

results induced by different types of septic shock in transglutaminase 2 knockout mice. Amino acids. 2013;44(1):189-97.
28. Yan Y, Kolachala V, Dalmasso G, Nguyen H, Laroui H, Sitaraman SV, et al. Temporal and spatial analysis of clinical and molecular parameters in dextran sodium sulfate induced colitis. PLoS One. 2009;4(6):e6073.
29. Grivennikov S, Karin E, Terzic J, Mucida D, Yu GY, Vallabhapurapu S, et al. IL-6 and Stat3 are required for survival of intestinal epithelial cells and development of colitis-associated cancer. Cancer cell. 2009;15(2):103-13.
30. Naito Y, Takagi T, Uchiyama K, Kuroda M, Kokura S, Ichikawa H, et al. Reduced intestinal inflammation induced by dextran sodium sulfate in interleukin-6-deficient mice. International journal of molecular medicine. 2004;14(2):191-6.
31. Sommer J, Engelowski E, Baran P, Garbers C, Floss DM, Scheller J. Interleukin-6, but not the interleukin-6 receptor plays a role in recovery from dextran sodium sulfate-induced colitis. International journal of molecular medicine. 2014;34(3):651-60.
32. Mudter J, Neurath MF. Il-6 signaling in inflammatory bowel disease: pathophysiological role and clinical relevance. Inflamm Bowel Dis. 2007;13(8):1016-23.
33. Jin X, Stamnaes J, Klock C, DiRaimondo TR, Sollid LM, Khosla C. Activation of extracellular transglutaminase 2 by thioredoxin. The Journal of biological chemistry. 2011;286(43):37866-73.
34. Diraimondo TR, Klock C, Khosla C. Interferon-gamma activates transglutaminase 2 via a phosphatidylinositol-3-kinase-dependent pathway: implications for celiac sprue therapy. J Pharmacol Exp Ther. 2012;341(1):104-14.
35. Ranganathan P, Jayakumar C, Manicassamy S, Ramesh G. CXCR2 knockout mice are protected against DSS-colitis-induced acute kidney injury and inflammation. American journal of physiology Renal physiology. 2013;305(10):F1422-7.
36. Noti M, Corazza N, Mueller C, Berger B, Brunner T. TNF suppresses acute intestinal inflammation by inducing local glucocorticoid synthesis. The Journal of experimental medicine. 2010;207(5):1057-66.
37. Kuhn R, Lohler J, Rennick D, Rajewsky K, Muller W. Interleukin-10-deficient mice develop chronic enterocolitis. Cell. 1993;75(2):263-74.
38. Li B, Alli R, Vogel P, Geiger TL. IL-10 modulates DSS-induced colitis through a macrophage-ROS-NO axis. Mucosal immunology. 2014;7(4):869-78.
39. Correa I, Veny M, Esteller M, Pique JM, Yague J, Panes J, et al. Defective IL-10 production in severe phenotypes of Crohn's disease. Journal of leukocyte biology. 2009;85(5):896-903.
40. Franke A, Balschun T, Karlsen TH, Sventoraityte J, Nikolaus S, Mayr G, et al. Sequence variants in IL10, ARPC2 and multiple other loci

contribute to ulcerative colitis susceptibility. Nature genetics. 2008;40(11):1319-23.
41. Kinugasa T, Sakaguchi T, Gu X, Reinecker HC. Claudins regulate the intestinal barrier in response to immune mediators. Gastroenterology. 2000;118(6):1001-11.
42. Ogawa A, Andoh A, Araki Y, Bamba T, Fujiyama Y. Neutralization of interleukin-17 aggravates dextran sulfate sodium-induced colitis in mice. Clinical immunology. 2004;110(1):55-62.
43. Yang XO, Chang SH, Park H, Nurieva R, Shah B, Acero L, et al. Regulation of inflammatory responses by IL-17F. The Journal of experimental medicine. 2008;205(5):1063-75.
44. O'Connor W, Jr., Kamanaka M, Booth CJ, Town T, Nakae S, Iwakura Y, et al. A protective function for interleukin 17A in T cell-mediated intestinal inflammation. Nature immunology. 2009;10(6):603-9.
45. Hueber W, Sands BE, Lewitzky S, Vandemeulebroecke M, Reinisch W, Higgins PD, et al. Secukinumab, a human anti-IL-17A monoclonal antibody, for moderate to severe Crohn's disease: unexpected results of a randomised, double-blind placebo-controlled trial. Gut. 2012;61(12):1693-700.
46. Nardacci R, Lo Iacono O, Ciccosanti F, Falasca L, Addesso M, Amendola A, et al. Transglutaminase type II plays a protective role in hepatic injury. The American journal of pathology. 2003;162(4):1293-303.
47. Perse M, Cerar A. Dextran sodium sulphate colitis mouse model: traps and tricks. Journal of biomedicine & biotechnology. 2012;2012:718617.
48. Kitajima S, Takuma S, Morimoto M. Tissue distribution of dextran sulfate sodium (DSS) in the acute phase of murine DSS-induced colitis. J Vet Med Sci. 1999;61(1):67-70.
49. Szondy Z, Sarang Z, Molnar P, Nemeth T, Piacentini M, Mastroberardino PG, et al. Transglutaminase 2-/- mice reveal a phagocytosis-associated crosstalk between macrophages and apoptotic cells. Proc Natl Acad Sci U S A. 2003;100(13):7812-7.
50. Balajthy Z, Csomos K, Vamosi G, Szanto A, Lanotte M, Fesus L. Tissue-transglutaminase contributes to neutrophil granulocyte differentiation and functions. Blood. 2006;108(6):2045-54.
51. Yin S, Gao B. Toll-like receptor 3 in liver diseases. Gastroenterol Res Pract. 2010;2010.
52. Field R, Campion S, Warren C, Murray C, Cunningham C. Systemic challenge with the TLR3 agonist poly I:C induces amplified IFNalpha/beta and IL-1beta responses in the diseased brain and exacerbates chronic neurodegeneration. Brain Behav Immun. 2010;24(6):996-1007.
53. Buford TW, Anton SD, Judge AR, Marzetti E, Wohlgemuth SE, Carter CS, et al. Models of accelerated sarcopenia: critical pieces for solving the puzzle of age-related muscle atrophy. Ageing research

reviews. 2010;9(4):369-83.
54. Marzetti E, Leeuwenburgh C. Skeletal muscle apoptosis, sarcopenia and frailty at old age. Experimental gerontology. 2006;41(12):1234-8.
55. Di Iorio A, Abate M, Di Renzo D, Russolillo A, Battaglini C, Ripari P, et al. Sarcopenia: age-related skeletal muscle changes from determinants to physical disability. International journal of immunopathology and pharmacology. 2006;19(4):703-19.
56. Hepple RT. Sarcopenia--a critical perspective. Science of aging knowledge environment : SAGE KE. 2003;2003(46):pe31.
57. Pitzalis C, Pipitone N, Bajocchi G, Hall M, Goulding N, Lee A, et al. Corticosteroids inhibit lymphocyte binding to endothelium and intercellular adhesion: an additional mechanism for their anti-inflammatory and immunosuppressive effect. J Immunol. 1997;158(10):5007-16.
58. Wheller SK, Perretti M. Dexamethasone inhibits cytokine-induced intercellular adhesion molecule-1 up-regulation on endothelial cell lines. European journal of pharmacology. 1997;331(1):65-71.
59. Bourke E, Moynagh PN. Antiinflammatory effects of glucocorticoids in brain cells, independent of NF-kappa B. J Immunol. 1999;163(4):2113-9.
60. Waddell DS, Baehr LM, van den Brandt J, Johnsen SA, Reichardt HM, Furlow JD, et al. The glucocorticoid receptor and FOXO1 synergistically activate the skeletal muscle atrophy-associated MuRF1 gene. American journal of physiology Endocrinology and metabolism. 2008;295(4):E785-97.
61. Glass DJ. Skeletal muscle hypertrophy and atrophy signaling pathways. The international journal of biochemistry & cell biology. 2005;37(10):1974-84.
62. Glass DJ. PI3 kinase regulation of skeletal muscle hypertrophy and atrophy. Current topics in microbiology and immunology. 2010;346:267-78.
63. Foletta VC, White LJ, Larsen AE, Leger B, Russell AP. The role and regulation of MAFbx/atrogin-1 and MuRF1 in skeletal muscle atrophy. Pflugers Archiv : European journal of physiology. 2011;461(3):325-35.
64. Shah OJ, Kimball SR, Jefferson LS. Acute attenuation of translation initiation and protein synthesis by glucocorticoids in skeletal muscle. American journal of physiology Endocrinology and metabolism. 2000;278(1):E76-82.
65. Molitoris JK, McColl KS, Swerdlow S, Matsuyama M, Lam M, Finkel TH, et al. Glucocorticoid elevation of dexamethasone-induced gene 2 (Dig2/RTP801/REDD1) protein mediates autophagy in lymphocytes. The Journal of biological chemistry. 2011;286(34):30181-9.
66. Shimizu N, Yoshikawa N, Ito N, Maruyama T, Suzuki Y, Takeda

S, et al. Crosstalk between glucocorticoid receptor and nutritional sensor mTOR in skeletal muscle. Cell metabolism. 2011;13(2):170-82.
67. Hansen CG, Nichols BJ. Exploring the caves: cavins, caveolins and caveolae. Trends in cell biology. 2010;20(4):177-86.
68. Kim HS, Kim HJ, Kim YS, Park SC, Harris R, Kim CK. Caveolin, GLUT4 and insulin receptor protein content in human arm and leg muscles. European journal of applied physiology. 2009;106(2):173-9.
69. Gazzerro E, Sotgia F, Bruno C, Lisanti MP, Minetti C. Caveolinopathies: from the biology of caveolin-3 to human diseases. European journal of human genetics : EJHG. 2010;18(2):137-45.
70. Scherer PE, Okamoto T, Chun M, Nishimoto I, Lodish HF, Lisanti MP. Identification, sequence, and expression of caveolin-2 defines a caveolin gene family. Proceedings of the National Academy of Sciences of the United States of America. 1996;93(1):131-5.
71. Drab M, Verkade P, Elger M, Kasper M, Lohn M, Lauterbach B, et al. Loss of caveolae, vascular dysfunction, and pulmonary defects in caveolin-1 gene-disrupted mice. Science. 2001;293(5539):2449-52.
72. Zhao YY, Liu Y, Stan RV, Fan L, Gu Y, Dalton N, et al. Defects in caveolin-1 cause dilated cardiomyopathy and pulmonary hypertension in knockout mice. Proceedings of the National Academy of Sciences of the United States of America. 2002;99(17):11375-80.
73. Kim HP, Wang X, Nakao A, Kim SI, Murase N, Choi ME, et al. Caveolin-1 expression by means of p38beta mitogen-activated protein kinase mediates the antiproliferative effect of carbon monoxide. Proceedings of the National Academy of Sciences of the United States of America. 2005;102(32):11319-24.
74. Oh YS, Khil LY, Cho KA, Ryu SJ, Ha MK, Cheon GJ, et al. A potential role for skeletal muscle caveolin-1 as an insulin sensitivity modulator in ageing-dependent non-obese type 2 diabetes: studies in a new mouse model. Diabetologia. 2008;51(6):1025-34.
75. Kawabe JI, Grant BS, Yamamoto M, Schwencke C, Okumura S, Ishikawa Y. Changes in caveolin subtype protein expression in aging rat organs. Molecular and cellular endocrinology. 2001;176(1-2):91-5.
76. Razani B, Combs TP, Wang XB, Frank PG, Park DS, Russell RG, et al. Caveolin-1-deficient mice are lean, resistant to diet-induced obesity, and show hypertriglyceridemia with adipocyte abnormalities. The Journal of biological chemistry. 2002;277(10):8635-47.
77. Oh YS, Lee TS, Cheon GJ, Jang IS, Jun HS, Park SC. Modulation of insulin sensitivity and caveolin-1 expression by orchidectomy in a nonobese type 2 diabetes animal model. Molecular medicine. 2011;17(1-2):4-11.
78. Oh YS, Kim HJ, Ryu SJ, Cho KA, Park YS, Park H, et al. Exercise type and muscle fiber specific induction of caveolin-1 expression for insulin sensitivity of skeletal muscle. Experimental & molecular medicine. 2007;39(3):395-401.
79. Pereira RM, Freire de Carvalho J. Glucocorticoid-induced

myopathy. Joint, bone, spine : revue du rhumatisme. 2011;78(1):41-4.
80. Baehr LM, Furlow JD, Bodine SC. Muscle sparing in muscle RING finger 1 null mice: response to synthetic glucocorticoids. The Journal of physiology. 2011;589(Pt 19):4759-76.
81. Schakman O, Gilson H, Thissen JP. Mechanisms of glucocorticoid-induced myopathy. The Journal of endocrinology. 2008;197(1):1-10.
82. Menconi M, Fareed M, O'Neal P, Poylin V, Wei W, Hasselgren PO. Role of glucocorticoids in the molecular regulation of muscle wasting. Critical care medicine. 2007;35(9 Suppl):S602-8.
83. Boscher C, Nabi IR. Caveolin-1: role in cell signaling. Advances in experimental medicine and biology. 2012;729:29-50.
84. Zhao W, Qin W, Pan J, Wu Y, Bauman WA, Cardozo C. Dependence of dexamethasone-induced Akt/FOXO1 signaling, upregulation of MAFbx, and protein catabolism upon the glucocorticoid receptor. Biochem Biophys Res Commun. 2009;378(3):668-72.
85. Schoneveld OJ, Gaemers IC, Lamers WH. Mechanisms of glucocorticoid signalling. Biochim Biophys Acta. 2004;1680(2):114-28.
86. Zheng B, Ohkawa S, Li H, Roberts-Wilson TK, Price SR. FOXO3a mediates signaling crosstalk that coordinates ubiquitin and atrogin-1/MAFbx expression during glucocorticoid-induced skeletal muscle atrophy. FASEB journal : official publication of the Federation of American Societies for Experimental Biology. 2010;24(8):2660-9.
87. Dostert A, Heinzel T. Negative glucocorticoid receptor response elements and their role in glucocorticoid action. Current pharmaceutical design. 2004;10(23):2807-16.
88. van Batenburg MF, Li H, Polman JA, Lachize S, Datson NA, Bussemaker HJ, et al. Paired hormone response elements predict caveolin-1 as a glucocorticoid target gene. PloS one. 2010;5(1):e8839.
89. Turney MK, Kovacs WJ. Function of a truncated glucocorticoid receptor form at a negative glucocorticoid response element in the proopiomelanocortin gene. Journal of molecular endocrinology. 2001;26(1):43-9.
90. Oshikawa J, Otsu K, Toya Y, Tsunematsu T, Hankins R, Kawabe J, et al. Insulin resistance in skeletal muscles of caveolin-3-null mice. Proceedings of the National Academy of Sciences of the United States of America. 2004;101(34):12670-5.
91. Ohsawa Y, Toko H, Katsura M, Morimoto K, Yamada H, Ichikawa Y, et al. Overexpression of P104L mutant caveolin-3 in mice develops hypertrophic cardiomyopathy with enhanced contractility in association with increased endothelial nitric oxide synthase activity. Human molecular genetics. 2004;13(2):151-7.
92. Galbiati F, Volonte D, Minetti C, Chu JB, Lisanti MP. Phenotypic behavior of caveolin-3 mutations that cause autosomal dominant limb girdle muscular dystrophy (LGMD-1C). Retention of LGMD-1C caveolin-3 mutants within the golgi complex. The Journal of biological

chemistry. 1999;274(36):25632-41.
93. Cohen AW, Hnasko R, Schubert W, Lisanti MP. Role of caveolae and caveolins in health and disease. Physiological reviews. 2004;84(4):1341-79.
94. Cohen AW, Combs TP, Scherer PE, Lisanti MP. Role of caveolin and caveolae in insulin signaling and diabetes. American journal of physiology Endocrinology and metabolism. 2003;285(6):E1151-60.
95. Schubert W, Sotgia F, Cohen AW, Capozza F, Bonuccelli G, Bruno C, et al. Caveolin-1(-/-)- and caveolin-2(-/-)-deficient mice both display numerous skeletal muscle abnormalities, with tubular aggregate formation. The American journal of pathology. 2007;170(1):316-33.
96. Razani B, Engelman JA, Wang XB, Schubert W, Zhang XL, Marks CB, et al. Caveolin-1 null mice are viable but show evidence of hyperproliferative and vascular abnormalities. The Journal of biological chemistry. 2001;276(41):38121-38.
97. Brooks SV. Current topics for teaching skeletal muscle physiology. Adv Physiol Educ. 2003;27(1-4):171-82.
98. Smerdu V, Karsch-Mizrachi I, Campione M, Leinwand L, Schiaffino S. Type IIx myosin heavy chain transcripts are expressed in type IIb fibers of human skeletal muscle. Am J Physiol. 1994;267(6 Pt 1):C1723-8.
99. Chin ER, Allen DG. The role of elevations in intracellular [Ca2+] in the development of low frequency fatigue in mouse single muscle fibres. J Physiol. 1996;491 (Pt 3):813-24.
100. Spangenburg EE, Booth FW. Molecular regulation of individual skeletal muscle fibre types. Acta Physiol Scand. 2003;178(4):413-24.
101. Chin ER, Olson EN, Richardson JA, Yang Q, Humphries C, Shelton JM, et al. A calcineurin-dependent transcriptional pathway controls skeletal muscle fiber type. Genes Dev. 1998;12(16):2499-509.
102. Vyas DR, McCarthy JJ, Tsika GL, Tsika RW. Multiprotein complex formation at the beta myosin heavy chain distal muscle CAT element correlates with slow muscle expression but not mechanical overload responsiveness. J Biol Chem. 2001;276(2):1173-84.
103. Baldwin KM, Klinkerfuss GH, Terjung RL, Mole PA, Holloszy JO. Respiratory capacity of white, red, and intermediate muscle: adaptative response to exercise. Am J Physiol. 1972;222(2):373-8.
104. Essen B, Jansson E, Henriksson J, Taylor AW, Saltin B. Metabolic characteristics of fibre types in human skeletal muscle. Acta Physiol Scand. 1975;95(2):153-65.
105. Schiaffino S. Fibre types in skeletal muscle: a personal account. Acta Physiol (Oxf). 2010;199(4):451-63.
106. Bergeron R, Ren JM, Cadman KS, Moore IK, Perret P, Pypaert M, et al. Chronic activation of AMP kinase results in NRF-1 activation and mitochondrial biogenesis. Am J Physiol Endocrinol Metab. 2001;281(6):E1340-6.

107. Wu Z, Puigserver P, Andersson U, Zhang C, Adelmant G, Mootha V, et al. Mechanisms controlling mitochondrial biogenesis and respiration through the thermogenic coactivator PGC-1. Cell. 1999;98(1):115-24.
108. Lin J, Wu H, Tarr PT, Zhang CY, Wu Z, Boss O, et al. Transcriptional co-activator PGC-1 alpha drives the formation of slow-twitch muscle fibres. Nature. 2002;418(6899):797-801.
109. Nakayama M, Stauffer J, Cheng J, Banerjee-Basu S, Wawrousek E, Buonanno A. Common core sequences are found in skeletal muscle slow- and fast-fiber-type-specific regulatory elements. Mol Cell Biol. 1996;16(5):2408-17.
110. Homsher E. Muscle enthalpy production and its relationship to actomyosin ATPase. Annu Rev Physiol. 1987;49:673-90.
111. Sahlin K, Tonkonogi M, Soderlund K. Energy supply and muscle fatigue in humans. Acta Physiol Scand. 1998;162(3):261-6.
112. Westerblad H, Bruton JD, Katz A. Skeletal muscle: energy metabolism, fiber types, fatigue and adaptability. Exp Cell Res. 2010;316(18):3093-9.
113. Zhang SJ, Sandstrom ME, Aydin J, Westerblad H, Wieringa B, Katz A. Activation of glucose transport and AMP-activated protein kinase during muscle contraction in adenylate kinase-1 knockout mice. Acta Physiol (Oxf). 2008;192(3):413-20.
114. Katz A, Sahlin K. Regulation of lactic acid production during exercise. J Appl Physiol (1985). 1988;65(2):509-18.
115. Holloszy JO. A forty-year memoir of research on the regulation of glucose transport into muscle. Am J Physiol Endocrinol Metab. 2003;284(3):E453-67.
116. Sandstrom ME, Zhang SJ, Bruton J, Silva JP, Reid MB, Westerblad H, et al. Role of reactive oxygen species in contraction-mediated glucose transport in mouse skeletal muscle. J Physiol. 2006;575(Pt 1):251-62.
117. McGlory C, Phillips SM. Exercise and the Regulation of Skeletal Muscle Hypertrophy. Prog Mol Biol Transl Sci. 2015;135:153-73.
118. Marcotte GR, West DW, Baar K. The molecular basis for load-induced skeletal muscle hypertrophy. Calcif Tissue Int. 2015;96(3):196-210.
119. Goldberg AL. Protein synthesis during work-induced growth of skeletal muscle. J Cell Biol. 1968;36(3):653-8.
120. Konopka AR, Harber MP. Skeletal muscle hypertrophy after aerobic exercise training. Exerc Sport Sci Rev. 2014;42(2):53-61.
121. Booth FW, Thomason DB. Molecular and cellular adaptation of muscle in response to exercise: perspectives of various models. Physiol Rev. 1991;71(2):541-85.
122. Pilegaard H, Saltin B, Neufer PD. Exercise induces transient transcriptional activation of the PGC-1alpha gene in human skeletal muscle. J Physiol. 2003;546(Pt 3):851-8.
123. Rockl KS, Witczak CA, Goodyear LJ. Signaling mechanisms in

skeletal muscle: acute responses and chronic adaptations to exercise. IUBMB Life. 2008;60(3):145-53.
124. Akimoto T, Pohnert SC, Li P, Zhang M, Gumbs C, Rosenberg PB, et al. Exercise stimulates Pgc-1alpha transcription in skeletal muscle through activation of the p38 MAPK pathway. J Biol Chem. 2005;280(20):19587-93.
125. Chen ZP, Stephens TJ, Murthy S, Canny BJ, Hargreaves M, Witters LA, et al. Effect of exercise intensity on skeletal muscle AMPK signaling in humans. Diabetes. 2003;52(9):2205-12.
126. Jacobs BL, You JS, Frey JW, Goodman CA, Gundermann DM, Hornberger TA. Eccentric contractions increase the phosphorylation of tuberous sclerosis complex-2 (TSC2) and alter the targeting of TSC2 and the mechanistic target of rapamycin to the lysosome. J Physiol. 2013;591(18):4611-20.
127. Baldwin KM, Haddad F. Skeletal muscle plasticity: cellular and molecular responses to altered physical activity paradigms. Am J Phys Med Rehabil. 2002;81(11 Suppl):S40-51.
128. Alessi DR, Cohen P. Mechanism of activation and function of protein kinase B. Curr Opin Genet Dev. 1998;8(1):55-62.
129. Hara K, Yonezawa K, Kozlowski MT, Sugimoto T, Andrabi K, Weng QP, et al. Regulation of eIF-4E BP1 phosphorylation by mTOR. J Biol Chem. 1997;272(42):26457-63.
130. Youtani T, Tomoo K, Ishida T, Miyoshi H, Miura K. Regulation of human eIF4E by 4E-BP1: binding analysis using surface plasmon resonance. IUBMB Life. 2000;49(1):27-31.
131. Hu SI, Katz M, Chin S, Qi X, Cruz J, Ibebunjo C, et al. MNK2 inhibits eIF4G activation through a pathway involving serine-arginine-rich protein kinase in skeletal muscle. Sci Signal. 2012;5(211):ra14.
132. Wang X, Yue P, Chan CB, Ye K, Ueda T, Watanabe-Fukunaga R, et al. Inhibition of mammalian target of rapamycin induces phosphatidylinositol 3-kinase-dependent and Mnk-mediated eukaryotic translation initiation factor 4E phosphorylation. Mol Cell Biol. 2007;27(21):7405-13.
133. Brown MC, Dobrikov MI, Gromeier M. Mitogen-activated protein kinase-interacting kinase regulates mTOR/AKT signaling and controls the serine/arginine-rich protein kinase-responsive type 1 internal ribosome entry site-mediated translation and viral oncolysis. J Virol. 2014;88(22):13149-60.
134. Welsh GI, Miller CM, Loughlin AJ, Price NT, Proud CG. Regulation of eukaryotic initiation factor eIF2B: glycogen synthase kinase-3 phosphorylates a conserved serine which undergoes dephosphorylation in response to insulin. FEBS Lett. 1998;421(2):125-30.
135. Neal JW, Clipstone NA. Glycogen synthase kinase-3 inhibits the DNA binding activity of NFATc. J Biol Chem. 2001;276(5):3666-73.
136. Berdeaux R, Stewart R. cAMP signaling in skeletal muscle

adaptation: hypertrophy, metabolism, and regeneration. Am J Physiol Endocrinol Metab. 2012;303(1):E1-17.
137. Hall RA, Lefkowitz RJ. Regulation of G protein-coupled receptor signaling by scaffold proteins. Circ Res. 2002;91(8):672-80.
138. Wauson EM, Zaganjor E, Lee AY, Guerra ML, Ghosh AB, Bookout AL, et al. The G protein-coupled taste receptor T1R1/T1R3 regulates mTORC1 and autophagy. Mol Cell. 2012;47(6):851-62.
139. Kimball SR, Jefferson LS. Signaling pathways and molecular mechanisms through which branched-chain amino acids mediate translational control of protein synthesis. J Nutr. 2006;136(1 Suppl):227S-31S.
140. Tatpati LL, Irving BA, Tom A, Bigelow ML, Klaus K, Short KR, et al. The effect of branched chain amino acids on skeletal muscle mitochondrial function in young and elderly adults. J Clin Endocrinol Metab. 2010;95(2):894-902.
141. Hasselgren PO, Fischer JE. The ubiquitin-proteasome pathway: review of a novel intracellular mechanism of muscle protein breakdown during sepsis and other catabolic conditions. Ann Surg. 1997;225(3):307-16.
142. Tiao G, Hobler S, Wang JJ, Meyer TA, Luchette FA, Fischer JE, et al. Sepsis is associated with increased mRNAs of the ubiquitin-proteasome proteolytic pathway in human skeletal muscle. J Clin Invest. 1997;99(2):163-8.
143. Jagoe RT, Goldberg AL. What do we really know about the ubiquitin-proteasome pathway in muscle atrophy? Curr Opin Clin Nutr Metab Care. 2001;4(3):183-90.
144. Powers SK, Kavazis AN, McClung JM. Oxidative stress and disuse muscle atrophy. J Appl Physiol (1985). 2007;102(6):2389-97.
145. Powers SK, Smuder AJ, Criswell DS. Mechanistic links between oxidative stress and disuse muscle atrophy. Antioxid Redox Signal. 2011;15(9):2519-28.
146. Jackman RW, Kandarian SC. The molecular basis of skeletal muscle atrophy. Am J Physiol Cell Physiol. 2004;287(4):C834-43.
147. Goll DE, Thompson VF, Li H, Wei W, Cong J. The calpain system. Physiol Rev. 2003;83(3):731-801.
148. Moldoveanu T, Jia Z, Davies PL. Calpain activation by cooperative Ca2+ binding at two non-EF-hand sites. J Biol Chem. 2004;279(7):6106-14.
149. Reverter D, Sorimachi H, Bode W. The structure of calcium-free human m-calpain: implications for calcium activation and function. Trends Cardiovasc Med. 2001;11(6):222-9.
150. Bartoli M, Richard I. Calpains in muscle wasting. Int J Biochem Cell Biol. 2005;37(10):2115-33.
151. Arthur JS, Crawford C. Investigation of the interaction of m-calpain with phospholipids: calpain-phospholipid interactions. Biochim Biophys Acta. 1996;1293(2):201-6.

152. Xiao YY, Wang MC, Purintrapiban J, Forsberg NE. Roles of mu-calpain in cultured L8 muscle cells: application of a skeletal muscle-specific gene expression system. Comp Biochem Physiol C Toxicol Pharmacol. 2003;134(4):439-50.
153. Purintrapiban J, Wang MC, Forsberg NE. Degradation of sarcomeric and cytoskeletal proteins in cultured skeletal muscle cells. Comp Biochem Physiol B Biochem Mol Biol. 2003;136(3):393-401.
154. Attaix D, Combaret L, Bechet D, Taillandier D. Role of the ubiquitin-proteasome pathway in muscle atrophy in cachexia. Curr Opin Support Palliat Care. 2008;2(4):262-6.
155. Vazeille E, Codran A, Claustre A, Averous J, Listrat A, Bechet D, et al. The ubiquitin-proteasome and the mitochondria-associated apoptotic pathways are sequentially downregulated during recovery after immobilization-induced muscle atrophy. Am J Physiol Endocrinol Metab. 2008;295(5):E1181-90.
156. Smalle J, Vierstra RD. The ubiquitin 26S proteasome proteolytic pathway. Annu Rev Plant Biol. 2004;55:555-90.
157. Bonaldo P, Sandri M. Cellular and molecular mechanisms of muscle atrophy. Dis Model Mech. 2013;6(1):25-39.
158. Vainshtein A, Grumati P, Sandri M, Bonaldo P. Skeletal muscle, autophagy, and physical activity: the menage a trois of metabolic regulation in health and disease. J Mol Med (Berl). 2014;92(2):127-37.
159. Lagirand-Cantaloube J, Cornille K, Csibi A, Batonnet-Pichon S, Leibovitch MP, Leibovitch SA. Inhibition of atrogin-1/MAFbx mediated MyoD proteolysis prevents skeletal muscle atrophy in vivo. PLoS One. 2009;4(3):e4973.
160. Csibi A, Leibovitch MP, Cornille K, Tintignac LA, Leibovitch SA. MAFbx/Atrogin-1 controls the activity of the initiation factor eIF3-f in skeletal muscle atrophy by targeting multiple C-terminal lysines. J Biol Chem. 2009;284(7):4413-21.
161. Clarke BA, Drujan D, Willis MS, Murphy LO, Corpina RA, Burova E, et al. The E3 Ligase MuRF1 degrades myosin heavy chain protein in dexamethasone-treated skeletal muscle. Cell Metab. 2007;6(5):376-85.
162. Polge C, Heng AE, Jarzaguet M, Ventadour S, Claustre A, Combaret L, et al. Muscle actin is polyubiquitinylated in vitro and in vivo and targeted for breakdown by the E3 ligase MuRF1. FASEB J. 2011;25(11):3790-802.
163. Chen GQ, Lu KR, Yang YQ, Wang S, Bie MJ. [Effects of oxidative stress on MuRF1 expression in skeletal muscle of diabetic rats]. Sichuan Da Xue Xue Bao Yi Xue Ban. 2011;42(3):349-52.
164. Malavaki CJ, Sakkas GK, Mitrou GI, Kalyva A, Stefanidis I, Myburgh KH, et al. Skeletal muscle atrophy: disease-induced mechanisms may mask disuse atrophy. J Muscle Res Cell Motil. 2015;36(6):405-21.
165. Mourkioti F, Rosenthal N. NF-kappaB signaling in skeletal muscle: prospects for intervention in muscle diseases. J Mol Med (Berl).

2008;86(7):747-59.
166. Hadian K, Krappmann D. Signals from the nucleus: activation of NF-kappaB by cytosolic ATM in the DNA damage response. Sci Signal. 2011;4(156):pe2.
167. Li YP, Chen Y, John J, Moylan J, Jin B, Mann DL, et al. TNF-alpha acts via p38 MAPK to stimulate expression of the ubiquitin ligase atrogin1/MAFbx in skeletal muscle. FASEB J. 2005;19(3):362-70.
168. Kim J, Won KJ, Lee HM, Hwang BY, Bae YM, Choi WS, et al. p38 MAPK Participates in Muscle-Specific RING Finger 1-Mediated Atrophy in Cast-Immobilized Rat Gastrocnemius Muscle. Korean J Physiol Pharmacol. 2009;13(6):491-6.
169. Kirschke H, Wiederanders B. Lysosomal proteinases. Acta Histochem. 1987;82(1):2-4.
170. Hasilik A. The early and late processing of lysosomal enzymes: proteolysis and compartmentation. Experientia. 1992;48(2):130-51.
171. Ralston E, Lu Z, Ploug T. The organization of the Golgi complex and microtubules in skeletal muscle is fiber type-dependent. J Neurosci. 1999;19(24):10694-705.
172. Bando Y, Kominami E, Katunuma N. Purification and tissue distribution of rat cathepsin L. J Biochem. 1986;100(1):35-42.
173. Capel F, Prod'homme M, Bechet D, Taillandier D, Balage M, Attaix D, et al. Lysosomal and proteasome-dependent proteolysis are differentially regulated by insulin and/or amino acids following feeding in young, mature and old rats. J Nutr Biochem. 2009;20(8):570-6.
174. Matsukura U, Okitani A, Nishimuro T, Kato H. Mode of degradation of myofibrillar proteins by an endogenous protease, cathepsin L. Biochim Biophys Acta. 1981;662(1):41-7.
175. Bosutti A, Toigo G, Ciocchi B, Situlin R, Guarnieri G, Biolo G. Regulation of muscle cathepsin B proteolytic activity in protein-depleted patients with chronic diseases. Clin Nutr. 2002;21(5):373-8.
176. Borsook H, Deasy CL, et al. The incorporation of labeled lysine into the proteins of guinea pig liver homogenate. J Biol Chem. 1949;179(2):689-704.
177. Mycek MJ, Clarke DD, Neidle A, Waelsch H. Amine incorporation into insulin as catalyzed by transglutaminase. Arch Biochem Biophys. 1959;84:528-40.
178. Park D, Choi SS, Ha KS. Transglutaminase 2: a multi-functional protein in multiple subcellular compartments. Amino Acids. 2010;39(3):619-31.
179. Fesus L, Piacentini M. Transglutaminase 2: an enigmatic enzyme with diverse functions. Trends Biochem Sci. 2002;27(10):534-9.
180. O'Neill GM, Prasanna Murthy SN, Lorand L, Khanna R, Liu SC, Hanspal M, et al. Activation of transglutaminase in mu-calpain null erythrocytes. Biochem Biophys Res Commun. 2003;307(2):327-31.
181. Fesus L, Szondy Z. Transglutaminase 2 in the balance of cell death and survival. FEBS Lett. 2005;579(15):3297-302.

182. Sarang Z, Madi A, Koy C, Varga S, Glocker MO, Ucker DS, et al. Tissue transglutaminase (TG2) facilitates phosphatidylserine exposure and calpain activity in calcium-induced death of erythrocytes. Cell Death Differ. 2007;14(10):1842-4.
183. Collighan RJ, Griffin M. Transglutaminase 2 cross-linking of matrix proteins: biological significance and medical applications. Amino Acids. 2009;36(4):659-70.
184. Nakaoka H, Perez DM, Baek KJ, Das T, Husain A, Misono K, et al. Gh: a GTP-binding protein with transglutaminase activity and receptor signaling function. Science. 1994;264(5165):1593-6.
185. Siegel M, Khosla C. Transglutaminase 2 inhibitors and their therapeutic role in disease states. Pharmacol Ther. 2007;115(2):232-45.
186. Eckert RL, Kaartinen MT, Nurminskaya M, Belkin AM, Colak G, Johnson GV, et al. Transglutaminase regulation of cell function. Physiol Rev. 2014;94(2):383-417.
187. Bersten AM, Ahkong QF, Hallinan T, Nelson SJ, Lucy JA. Inhibition of the formation of myotubes in vitro by inhibitors of transglutaminase. Biochim Biophys Acta. 1983;762(3):429-36.
188. Huang YP, Seguro K, Motoki M, Tawada K. Cross-linking of contractile proteins from skeletal muscle by treatment with microbial transglutaminase. J Biochem. 1992;112(2):229-34.
189. Son YH, Lee SJ, Lee KB, Lee JH, Jeong EM, Chung SG, et al. Dexamethasone downregulates caveolin-1 causing muscle atrophy via inhibited insulin signaling. J Endocrinol. 2015;225(1):27-37.
190. Lopez-Bergami P, Kim H, Dewing A, Goydos J, Aaronson S, Ronai Z. c-Jun regulates phosphoinositide-dependent kinase 1 transcription: implication for Akt and protein kinase C activities and melanoma tumorigenesis. J Biol Chem. 2010;285(2):903-13.
191. Lira FS, Tavares FL, Yamashita AS, Koyama CH, Alves MJ, Caperuto EC, et al. Effect of endurance training upon lipid metabolism in the liver of cachectic tumour-bearing rats. Cell Biochem Funct. 2008;26(6):701-8.
192. Lerman I, Harrison BC, Freeman K, Hewett TE, Allen DL, Robbins J, et al. Genetic variability in forced and voluntary endurance exercise performance in seven inbred mouse strains. J Appl Physiol (1985). 2002;92(6):2245-55.
193. Silvestri C, Ligresti A, Di Marzo V. Peripheral effects of the endocannabinoid system in energy homeostasis: adipose tissue, liver and skeletal muscle. Rev Endocr Metab Disord. 2011;12(3):153-62.
194. Sakamoto A, Oda Y, Iwamoto Y, Tsuneyoshi M. A comparative study of fibrous dysplasia and osteofibrous dysplasia with regard to expressions of c-fos and c-jun products and bone matrix proteins: a clinicopathologic review and immunohistochemical study of c-fos, c-jun, type I collagen, osteonectin, osteopontin, and osteocalcin. Hum Pathol. 1999;30(12):1418-26.
195. Chen YR, Tan TH. The c-Jun N-terminal kinase pathway and

apoptotic signaling (review). Int J Oncol. 2000;16(4):651-62.
196. Ribera J, Ayala V, Casas C. Involvement of c-Jun-JNK pathways in the regulation of programmed cell death of developing chick embryo spinal cord motoneurons. Dev Neurosci. 2007;29(6):438-51.
197. Cheng CC, Hsueh CM, Liang KW, Ting CT, Wen CL, Hsu SL. Role of JNK and c-Jun signaling pathway in regulation of human serum paraoxonase 1 gene transcription by berberine in human HepG2 cells. Eur J Pharmacol. 2011;650(2-3):519-25.
198. Norlin M, Pettersson H, Tang W, Wikvall K. Androgen receptor-mediated regulation of the anti-atherogenic enzyme CYP27A1 involves the JNK/c-jun pathway. Arch Biochem Biophys. 2011;506(2):236-41.

초 록

트랜스글루타미네이즈 2 (TG2)는 단백질의 교결합, 폴리아미네이션, 탈아미드화와 같은 번역 후 변형 (post-translational modification)을 촉매하는 효소이다. TG2는 모든 조직 및 세포기관에서 발현하며, 백내장, 섬유증, 암과 같은 질병의 발병기전과 관련이 있다. 본 연구에선 아직 연구 되지 않은 급성장염과 근위축증에서 TG2의 역할을 구명하였다.

첫 번째 연구에서는 염증성장질환에서 TG2의 역할을 규명하였다. 최근, 블레오마이신으로 폐섬유를 유도한 동물에서, TG2가 T_H 17세포의 분화를 유도하여 염증을 유발한다고 알려졌다. 그러나, T_H 17세포와 의한 질병이라고 알려진 염증성 장 질환에서 TG2의 역할에 대한 연구는 이루어지지 않았다. 따라서 dextran sulfate sodium(DSS)으로 유도되는 급성 장염 모델을 이용하여 장염증 질환에서 TG2의 기능을 연구하였다. DSS를 섭취한 $TG2^{-/-}$ 생쥐는 야생형 생쥐와 비교할 때, 대장의 사이토카인, 몸무게, 장의 길이, 면역세포의 침범, 장의 흡수도에서 차이가 없었으나 $TG2^{-/-}$생쥐의 생존율이 현저히 낮았다. 이 결과는 DSS에 의하여 급성장염증이 유발되는 과정에서 TG2가 관련되어 있지 않으나, DSS의 독성에 대한 저항성과 관련이 있음을 보여준다.

두 번째 연구에서는 근위축증 모델에서 dexamethasone (DEX)에 의하여 저해되는 인슈린/IGF1 신호전달과정을 분석하였다. DEX처리한 C2C12 myotube에서 신호전달 단백질의 양을 분석한 결과, insulin receptor와 IRS1양이 감소하였는데, 이는 DEX에 의하여 caveolin1의 발현이 억제되기 때문이었다. 이 결과로 caveolin1이 스테로이드 호르몬의 타겟 유전자임을, 또한 caveolin1을 통하여 스테로이드 신호전달과 인슈린 신호전달과정이 연결되고 있음을 새로이 알게 되었다.

세 번째 연구에서는 TG2의 근위축증에서 역할을 구명하였다. $TG2^{-/-}$ 생쥐가 야생형 생쥐에 비해서 운동능력이 떨어짐을 관찰하였다. $TG2^{-/-}$생쥐의 몸무게, 비복근의 무게, 그리고 근육 fiber 크기를 측정하여, 비복근에서 근섬유의 크기가 유의적으로 감소된 것을 확인하였다. $TG2^{-/-}$생쥐 비복근에서 단백질 합성과 관련된 인슐린/IGF-1 신호전달 과정을 분석한

결과, 인슐린/IGF-1에 의해서 활성화되는 PI3K는 증가하는 반면에 그 하위 신호전달 물질인 PDK1의 단백질은 감소되어 있었다. C2C12 myotube에서 TG2의 억제제 및 siRNA는 PDK1유전자의 프로모터에서 c-Jun reporter 활성을 억제하였다. Western blot분석과 Real-time RT-PCR분석으로 TG2가 c-Jun의 전사에는 영향을 미치지 않지만, c-Jun의 분해를 억제하여 c-Jun단백질 양을 조절함을 알게 되었다. 이 결과는 TG2가 근육의 항상성을 유지하는데 필요함을 보여준다.

주요어: 트랜스글루타미네이즈 2, 근위축증, C2C12, 덱사메타손, 덱스트란 설페이트, 인슐린/IGF-1 신호전달
학번: 2009-31109